



TÉCNICO
LISBOA

Optical link budget for Low-Earth-Orbit satellite and high-altitude platforms for Quantum Key Distribution Missions

Ricardo Gil Atanásio de Carvalho

Thesis to obtain the Master of Science Degree in

Electrical and Computer Engineering

Supervisor(s): Professor Paulo Sérgio Brito André
Engenheiro Ricardo André Pinto Faria

Examination Committee

Chairperson: Professor José Eduardo Charters Ribeiro da Cunha Sanguino

Supervisor: Professor Paulo Sérgio Brito André

Member of the committee: Professor António Luis Campos da Silva Topa

November 2021

Declaration

I declare that this document is an original work of my own authorship and that it fulfills all the requirements of the Code of Conduct and Good Practices of the Universidade de Lisboa.

To my family and friends...

Acknowledgments

The author would like to express his sincere gratitude to Professor Paulo André for the continuous support during this thesis, for his patience, dedication, knowledge and guidance.

To the Quantum Team at Capgemini Engineering, in particular to Ricardo Faria, Preeti Yadav and André Gabriel, for their knowledge, experience and guidance in the making of this thesis.

A special thanks to the author's parents, sister and friends, for their unconditional encouragement and support during this journey.

And finally to Instituto Superior Técnico (IST), a school filled with scientific knowledge, where the author completed his studies.

Resumo

As comunicações por satélite com distribuição de chaves quânticas estão a tornar-se cada vez mais importantes hoje em dia porque oferecem uma maneira de transmitir informação entre dois pontos distantes de maneira muito rápida e segura. Com a distribuição de chaves quântica é possível compartilhar uma mensagem entre duas partes usando fibras ópticas ou ligações em espaço livre. Os sistemas de comunicação quântica usam a luz para transmitir fótons codificados quanticamente. Esses fótons codificados são então enviados para locais distantes. Por meio desse mecanismo de codificação e decodificação, duas partes distantes podem compartilhar uma string de bits aleatórios também chamados de chaves secretas, que podem ser usados para encriptar e desencriptar mensagens secretas. Embora esta seja uma tecnologia muito promissora e inovadora, ainda existem limitações e desafios que precisam de ser superados em relação às ligações em espaço livre. Algumas das dificuldades desta tecnologia têm a ver com a atenuação no canal óptico, principalmente devido à turbulência da atmosfera e à dificuldade em apontar um laser para uma plataforma em constante movimento. O QKD (Quantum Key Distribution) em fibras ópticas tem sido um tema de estudo durante muitos anos, porém a dificuldade em fazer chegar a fibra a locais remotos não o tornam uma tecnologia viável para compartilhar chaves secretas ao longo de grandes distâncias. Também as perdas ópticas do canal quântico em espaço livre são menores do que nas fibras ópticas, então o QKD em satélites tem sido considerado uma alternativa para distâncias maiores. O problema é que os custos de implementação e manutenção dos satélites são muito altos, portanto irá sempre haver uma barreira entre a tecnologia e o mercado. Outro método de explorar a tecnologia quântica em espaço livre é usando sistemas QKD em plataformas de elevada altitude (HAP's). Esta tecnologia ainda é muito nova e não existem muitos estudos que mostrem a viabilidade do uso de QKD em HAP's, então o principal objetivo desta tese é pesquisar e estudar um método ou sistema com parâmetros técnicos simulando resultados que permitam analisar vários factores que são necessários ter em consideração ao transmitir um sinal ótico no espaço.

Palavras-chave: Distribuição de chaves quânticas, Comunicações ópticas em espaço livre, plataformas de elevada altitude.

Abstract

Quantum key distribution with satellite communications are becoming more and more important nowadays because they offer a way to transmit information between two distant parties in a secure way. With Quantum Key Distribution (QKD) it's possible to share a message between two parties using fiber networks or free-space links. Quantum communication systems use photons that are encoded in a quantum state in physical degrees of freedom. These encoded photons are then sent to distant locations. Through this mechanism of encoding and decoding, two distant parties can share a string of random bits also called secret keys, which can be used to encrypt and decrypt secret messages. Although this is a very promising and innovative technology there are still limitations and challenges that need to be overcome. QKD, with both optical fibres and terrestrial free-space links, has been a case of study for many years, however, the difficult access to remote areas does not make it a feasible technology to share secret keys over large distances. The satellite-based QKD also offers smaller optical losses, so it has been considered as an alternative for large distances. The losses in a satellite-based optical channel are caused mainly due to the turbulence of the atmosphere and the difficulty of pointing a laser to a platform that is constantly moving. However, a issue with this solution is that the deployment and maintenance costs of satellites are very high so there will always be a barrier between the technology and the market. Another method of exploring the free space quantum technology is by using QKD systems on High Altitude Platforms (HAPs). This technology is still very recent and there are not many studies to show the feasibility of using QKD on HAPs so the main objective of this thesis is to research and study a method or system with technical parameters while simulating results that will allow achieving a QKD between Earth and HAPs.

Keywords: Quantum Key Distribution, Free Space Optics, High Altitude Platforms.

Chapter 1

Introduction

1.1 Motivation

Nowadays, the importance of transmitting information securely between two parties has become a very important issue. In today's world and in the future, data is one, if not the most important and valuable asset. In a few years time quantum computers will be able to crack any type of classical information being transmitted so the need for quantum encryption is a big necessity for sensitive data to be transmitted. Using QKD on satellites will overcome the challenge of the distances regarding optical fibers and terrestrial optical communications, with world wide coverage being a reality.

1.2 Topic Overview

Quantum key distribution has been a case of study for many years. QKD is a scheme for enabling two parties, commonly referred to as Alice and Bob to share a secret key between them. This sharing of information can be done using different quantum key distribution protocols. One of the protocols, the BB84 has the objective of encoding every bit of the the secret key into the polarization state of a single photon. Other very commonly used protocol is the E91 protocol that uses entangled pairs of photons. Using this protocol, Alice and Bob each receive one photon from each pair, either distributed by Alice or by a Satellite that sends the pair of photons to each of them using techniques to split a photon into two other photons of lower energy. These protocols will be better explained ahead. The idea is to be able to study a payload for the Altran EcoSat with reduced dimensions and mass that can carry a QKD system as well as comparing the differences between using a LEO satellite and a HAP. QKD in optical fibres has been a case of study for many years now, but experiments have shown that due to the exponential losses on optical fibres over large distances, long-distances secure key distribution in optical fibres becomes inefficient. In free space the quantum channel losses are much lower, so QKD via satellites has been considered as a feasible alternative to share keys over large distances. Despite amplification on optical fibers being an advantage that does not exist yet for satellites, it is not feasible to use optical fibers for the distances that are possible to achieve with a QKD in space. Many demonstrations have taken place that

show that QKD systems on satellites is a viable approach and has the potential to become a deployable service. However the difficulties of satellite operation and the high costs associated with maintenance in space make this technology a bigger barrier for the market.

As an alternative, one method of exploring free space quantum communication has to do with implementing QKD systems on HAPs. This is still a very recent approach because of the immature HAP technology and lack of global deployment capability. However some studies with HAP's have proven to be able to continuously provide commercial services such as 4G wireless communication services to remote areas by using a network of high altitude balloons. Using HAP's instead of LEO satellites for QKD systems brings both advantages and disadvantages. Satellites have predictable trajectories compared with HAP's, that despite being static have more random movements due to wind and atmospheric conditions, which need a coarse system, for example a gimble, to adjust to this random variations. However the smaller distances to the Earth provide much less optical attenuation and possible operation during daylight. The lower deployment and maintenance costs allow the QKD service to be accessible to a larger market. The long endurance of the HAP's allow QKD services to be delivered to certain regions continuously, unlike the unavoidable service window of the QKD on LEO satellites [1]. The following table summarizes the biggest differences in using HAP's and LEO satellites for QKD communications:

Table 2.2 - LEO vs HAP

HAP	LEO
HAPs deployment are at lower altitudes (20 km) when compared to LEO satellites, therefore leading to a favorable link budget with a high SNR.	LEO satellites are deployed at altitudes from 500 km to 2000 km, and the beam misalignment on the uplink is a major issue.
HAPs have almost stationary positions making the PAT (Pointing, Acquisition and Tracking) much easier.	On the contrary LEO satellites have a big orbital velocity which makes the PAT much more complicated.
The costs and risks of deploying a HAP is much more reduced when compared to a LEO satellite. Also HAP's are easy to bring back to Earth.	LEO satellites involve high deployment costs and are usually not recoverable.

1.3 Objectives

The main goal of this thesis is to compare and study the differences of using a HAP and a LEO satellite for QKD communication in space, and at the same time define the system SWaP (size, weight and power) parameters of a QKD payload that is suitable for using aboard a HAP or a LEO satellite in space. The main challenges to be addressed have to do with the turbulence of the optical channel, the pointing, acquisition and tracking, the coverage area and the available power for QKD after a certain distance.

1.4 Thesis Outline

In chapter 3 (Theoretical Overview) a study is done about all the aspects involved in free space optical communications. In sub-section 3.1 the theory about the coverage area, which is one of the most important parameters for satellite communications, is covered. In the next sub-section, 3.2, we can take a look into the BER, an important parameter for the performance of the optical receivers in a digital transmission system. In sub-section 3.3 a look into the Photodetectors is taken, which are used to convert the optical signal into an electrical signal. Sub-section 3.4 describes other very important aspect of FSO (free space optical communications) which is the pointing system, this is, the ability to track a laser sent from the transmitter to the receiver. In sub-section 3.5 the theory about one method to calculate the Link Budget analysis is calculated, taking into account the different factor that affect the optical channel. Finally in sub-section 3.6 and 3.7, it's studied a possible type of optical and quantum payload that could be used aboard a satellite or a HAP, and the different types of distributing photons between two parties. In the last chapter, 4, there are some results, which were obtained with a Python Script, about the coverage area, the link budget and the pointing system. The last sub section of chapter 4, sub-section 4.5, is a comparison between different models used by different authors to calculate the Link Budget.

Chapter 2

State of the Art

2.1 Free Space Optical Communication

Free space optical (FSO) is the designation of optical communication systems between two points in the air or vacuum, a receiver and a transmitter that are in LOS (Line-Of-Sight). FSO communications offer high data rate which concerning the tremendous demand for traffic nowadays is certainly a very important aspect to take into account. However, FSO is affected by atmospheric effects, such as turbulence, absorption and scattering, which limits the receiver sensitivity and therefore the bit error rate (BER) (Section 3.2). Due to the wide bandwidth and the narrow beam divergence, optical communication equipment require lower power supply than the traditional radio-frequency (RF), so optical transmitters and receivers are lightweight and small sized, resulting in a mass and space reduction in the satellites or base stations. Currently, FSO systems are capable to operate up to 2.5 Gbps of data, voice and video communications through the air, allowing optical connectivity without requiring fiber-optic cable or securing spectrum licenses. They operate between the 780 – 1600 nm spectrum region and use transponders to transform the optical signal into an electrical signal. In this band, high- performance transmitters and receivers are readily available in the market. Optical antennas have a very high gain which means that the size of the optical receiver can be very small since the power requirements are low. The use of smaller receivers, however, can make the pointing, acquisition and tracking (PAT) procedure to moving platforms more difficult.

Early experiments in FSO were demonstrated by Alexander Graham Bell which preceded the invention of the telephone. In his experiments, beams of light were used to transmit voice conversations through the air. These experiments were never used for commercial purposes but the principle of FSO was demonstrated. In 1880 Bell and his assistant Charles Tainter created the photo-phone. This device allowed the transmission of sound on a beam of light. Later on that same year, Bell conducted the world's first wireless telephone transmission between two buildings, 213 meters apart. Later on, in the early 60s and 70s, gas lasers and flash pumped solid-state lasers started to be used as transmitters for FSO, however they presented multiple problems regarding lifetime, size, weight and power. [2].

In the late 70s and early 80s semi conductor laser technology started to be a success and it was

demonstrated that they could be used in FSO. Despite these lasers promising to be very small, have high efficiency and have a large life span, there were a lot of challenges to overcome. At the time the European Space Agency (ESA) placed a technology research contract for the assessment of modulators for high data-rate laser links in space, which marked the beginning of ESA long involvement in space optical communications. With the fast evolution in the technology and interest in this topic, optical communications were being proposed and funded for air-to-air applications, satellite-to-submarine, air-to-submarine, air-to-satellite and satellite-to-satellite [3].

In the 80s both Europe and the United States increased dramatically their research in the FSO field. In Europe, ESA started a very promising project called the "Semi conductor laser inter satellite link experiment (SILEX) program". The SILEX program is a free-space optical communication system, which consists of two optical communication payloads aboard the ESA Advanced Relay and Technology Mission Satellite (ARTEMIS) spacecraft, optical payload for inter- satellite link experiment (OPALE), and on the French Earth-observation spacecraft SPOT-4, PASTEL. It allows data transmission of 50 Mbps from LEO (Low-Earth-orbit) to GEO (Geostationary Orbit) satellites using GaAlAs laser diodes and direct detection [3]. On the 20th of November of 2001, the laser link between ARTEMIS and SPOT-4 was successfully established. A 50 Mbps data rate between the transmitter and the receiver was successfully achieved. Then on the 30th of November, the first image was successfully transmitted via an inter-satellite link from SPOT-4 to ARTEMIS [3]. The success in this experiment was a milestone in the long and promising history of the development of optical space communications in EUROPE which is now becoming a very competitive market, specially regarding optical communications between LEO satellites and Earth.

The first successful LEO to Earth laser communication link was carried out in 2006 by a Japanese operator called JAXA, where they used LUCE (laser-utilizing communications equipment) aboard OICETS (optical inter-orbit communications engineering test satellite) a 570 kg satellite at a 610 km orbit. LUCE was a 100 kg payload based on a 2 axis gimballed 26 cm Cassegrain telescope with a transmitting power of 100 mW, an operating wavelength of 847 nm at 50 Mb/s, and with an accurate fine pointing system able to control the 5 cm footprint beam that reached the ground station where a 20 cm telescope was used to receive the incoming signal, coupling it into an APD [4].

In 2010, the United States Department of Defense launched the NFIRE (near-field infrared experiment) LEO satellite with Tesat's LCT (laser communications terminal) on board. Although the goal of this terminal was to carry out inter-satellite links, it was used for LEO to ground links as an experiment. The LCT payload consisted of a two axis gimballed mirror assembly fixed to a 12.5 cm telescope transmitting a 1 W 1064 nm laser at 5.6 Gb/s, using homodyne BPSK (binary phase-shift keying) with no beacon [4].

In 2011 China launched its first lasercom terminal LCE (laser communication equipment) into a 971 km LEO aboard the Haiyang-2A 1500 kg satellite. The payload was based on a 15 cm gimballed telescope with a 1 W power transmitting laser with a 1 μ rad tracking accuracy, achieving a maximum data rate of 504 Mb/s. In 2014 NASA installed the OPALS (optical payload lasercom science) terminal in the International Space Station (ISS), at a 408 km orbit. OPALS consists of a two-axis gimbal to move a 5 cm telescope and transmit a 2.5 W laser at 50 Mb/s. The high transmitting power enabled to relax the

pointing accuracy down to $300 \mu\text{rad}$, enough to point the 1mrad divergent beam to the ground station [4].

The first lasercom payload system aboard a small satellite (48 kg) was the SOTA (small optical transponder) from Japanese NICT's aboard SOCRATES, which was launched in May 2014 into a 628 km LEO orbit. SOTA was a two axis gimballed terminal weighting 6 kg, able to perform a variety of lasercom experiments. The core experiment was the 10 Mb/s links at 1549 nm using a pointing system to accurately transmit a 35 mW laser through a 5 cm Cassegrain telescope. SOTA had other additional capabilities such as a QKD payload implementing the B92 protocol at 800 nm band, performing the first quantum-limited demonstration from space, and 10 Mb/s downlinks at 980 nm using a small lens, both based on coarse pointing only. A collaboration with the Tohoku University, NICT developed a simplified version of SOTA named VSOTA (very small optical transponder) with a weight of less than 0.7 kg based only on body pointing, transmitting a 1550 nm laser beam with a wide divergence (1.3 mrad), low power (80 mW) at a low data rate (up to 1 Mb/s). VSOTA lost its launch opportunity planned for 2013 and was just launched in 2019. Based on SOTA and VSOTA, NICT is currently working towards the next generations of miniaturized high-speed lasercom transmitters compatible with CubeSat platforms for LEO-GEO inter-satellite links as well as LEO to ground links [4].

DLR (German Aerospace Center), in Germany, has been developing optical terminals for small satellites (CubeSats up to 100 kg) since 2008 in the 1550 nm wavelength based on COTS components to provide solutions to small satellites with reduced mass and power. In 2018 the first two generation of terminals that rely the pointing on the satellite attitude control (reducing the terminal mass to the 1 kg class) were launched, OSIRISv1 and OSIRISv2. The first generation OSIRISv1, was launched in July 2017 aboard the Flying Laptop satellite of the university of Stuttgart. DLR's OSIRIS aboard BIROS, known as OSIRISv2, was launched in June 2016 into a 500 km orbit, including an InGaAs 4-quadrant-tracking sensor to track the 1560 nm modulated beacon. The payload is designed for downlinks up to 1Gb/s using an OOK-modulated 1 W 1545 nm laser through a 1.5 cm lens with $200 \mu\text{rad}$ divergence angle. OSIRISv2 also includes another downlink capability up to 150 Mb/s using a different 1.5 cm lens with a divergence of $1200 \mu\text{rad}$ and transmitting power of 150 mW at 1550 nm [4].

In August 2016, the Chinese Academy of Sciences launched the Micius LEO satellite to a 500 km orbit whose primary mission was quantum communication experiments, but MCLCD (Micius coherent laser communication demonstration) was also planned. The MCLCD space terminal shared the main optics with the quantum experiment used to transmit a 2.2 W $40 \mu\text{rad}$ 1549 nm laser beam with a DPSK achieving a data rate of 5.12 Gb/s in 1.2 m Cassegrain telescope on the ground. The following table summarizes some of the LEO satellite experiments [4].

Table 1.1: LEO satellites experiments [4]

	LUCE	LCT	LCE	OPALS	SOTA	OSIRISv2	OSIRISv1	MCLCD
Satellite	OICETS (570 kg)	NFIRE (494kg)	Haiyang- 2A (1500kg)	ISS (420t)	SOCRATES (48kg)	BIROS (130kg)	Flying laptop (120kg)	Micius (631kg)
Launch Date	Aug 23, 2005	April 24, 2007	Aug 16, 2011	April 18, 2014	May 24, 2014	June 22, 2016	July 14, 2017	Aug 15, 2016
LEO alti- tude	610 km	495 km	971 km	408 km	628 km	500 km	600 km	500 km
Mass	100 kg	35 kg	67.8 kg	180 kg	5.9 kg	1.65 kg	1.34 kg	-
Max bitrate	50 Mb/s	5.6 Gb/s	504 Mb/s	50 Mb/s	10 Mb/s	1 Gb/s	200 Mb/s	5.12 Gb/s

2.2 QKD

The first implementation of a quantum key distribution in free space goes back to 1991, when H. Bennett, F. Bassett, G. Brassard, L. Salvail and J. Smolin [5] used a measure protocol about secret bits to share information between two parties, denominated Alice and Bob, using rectilinear basis (horizontal and vertical polarization) and circular basis (left circular and right circular polarization). In this experiment the signal was attenuated to an average of 0.1 photons per pulse. This was good to be demonstrated in short distances, but too weak to be used for greater distances due to the physical imperfections of the equipment and also the channel attenuation. Also the conversion efficiency of the detectors used (9%) limited the key rate transmission, resulting in over 715 000 pulses sent but only 4000 detected. On average, roughly half of the detections had the correct basis and the process took approximately 10 minutes. In this experiment the authors stated that without an eavesdropper the parties ended up with 754 bits of shared keys and with an eavesdropper this was reduced to 105 bits which left much room for improvement [6].

The first demonstration for a successful free space quantum key exchange in an outdoor environment was published in 1996 by C. Jacobs and J. D. Franson [7]. The approach was similar to the previous one, except that in this case diagonal polarization was used by adding a second Pockels Cell (an optical component that can change the light's polarization direction as a function of the applied voltage). The experiment was performed during the day and over 75 m. The single photon would travel through the air into an optical fiber with a small diameter of 3 μm , which prevented other sources of light into the system. Two silicon avalanche photodiodes were used with 50% efficiency and they achieved a transmission rate of 1 kHz [6].

The next big step in quantum key distribution was the experiment done by a group of physicists in the university of California at the Los Alamos National Laboratory in 1998 [5], they conducted the

experiment over a distance of 1 km using the B92 protocol. The maximum distance achieved in this experiment was 950 m under night time. An average photon number of ≤ 0.1 was used per pulse for transmission. The resulting BER was 1.5% which was lowered to 0.7% at a distance of 240 m. In this experiment a laser was used to generate a large number of photons (10^5) with a 1 ns optical pulse which was then attenuated to reach a 2-photon probability of less than 0.5% which implies that less than 6 of every 100 detectable pulses could contain 2 or more photons. The laser used had a wavelength of 772 nm. With the transmitter pulsed at 20kHz the achieved bit rate was of 50Hz . This experiment showed the feasibility of ground to satellite communication. The authors suggested that under nighttime a key generation rate of 35 to 450Hz was possible [6].

In 2002 the Los Alamos National Laboratory made improvements in their last experiment making a quantum key exchange over a distance of 9.81km in free space. This experiment was conducted during both day and night time. During the day the average photon number per pulse was between 0.2 and 0.8, whereas during the night it decreased to a value between 0.1 and 0.2, since the probability that the photon will be successfully detected also depends on the atmospheric transmission efficiency which varies under these aspects. Other important factor is the detection efficiency which is dependent on the physical characteristics of the optical receiver [6]. The BB84 protocol was used. In this experiment some of the parameters such as the wavelength were the same as the previous experiment. Here a cryptographic monolithic randomizer generates two random bits to determine which of the four temperature-controlled diode lasers will fire. Each laser corresponds to a state, either in the rectilinear or diagonal basis. The lasers emit a 1 ns, 772 nm optical pulse. On each cycle a 1 ns 1550 nm timing pulse was sent. The authors claim that this setup is both simple and secure, however the malfunction of the random generator could sabotage the integrity of the operation, with the eavesdropper being able to determine which laser was fired, resulting in discovering the whole key that is being transmitted. During this experiment

In 2006 a new experience with much larger transmission distances was performed by R. Ursin [8]. The polarization entangled photons were generated by Alice, 2400 m above sea level. A pico-second pulsed laser used with a special crystal created entangled photon pairs with a wavelength of 710 nm. The Ekbert Protocol was used. The photons are detected in rectilinear or diagonal bases. In this experiment one pair of photons is detected at Alice's side, and the other half is sent to Bob over a 144 km distance. The alignment was adjusted with a beacon laser based tracking system to mitigate beam wandering. The optical link efficiency was further attenuated by losses regarding diffraction, absorption and imperfections in the physical components. At these altitudes the losses were around 0.07 dB/km. The attenuation of the whole channel was -25 dB in the best case scenario with 25% single photon detection efficiency that was equivalent to 6 dB attenuation. On both sides each detection has a time tag that Bob sends to Alice who can then see which part of the message arrived to Bob. To check for the presence of entanglement, the evaluation on CHSH inequality is necessary and it's violation was confirmed. CHSH inequality can be used in the proof of Bell's theorem, which states that certain consequences of entanglement in quantum mechanics cannot be reproduced by local hidden variable theories – a local hidden-variable theory refers to all types of theory that attempt to account for the probabilistic features

of quantum mechanics by the mechanism of underlying inaccessible variables, with the additional requirements from local realism that distant events are independent, ruling out instantaneous interactions between separate events [9]. The experiment however violated the locality loophole to some extent since the detection of the first photon took place while the other photon was still just few meters away, nevertheless the detection of the other photon was still space-like separated. This resulted in 178 bits of secure key with a key rate of $2.3\text{bit}/s$. These rates are not enough for modern crypto systems, however it shows that it is possible to share a key over large distances which is very good since earth to satellite communications usually have a minimum distance of 400km for Low Earth Orbit satellites.

Satellite to ground communications are now a reality, however there are still challenges that need to be overcome. In 2012 this feasibility was demonstrated [10] with an aircraft to ground downlink FSO experiment from a moving airborne platform using the BB84 protocol. The experiment was conducted after sunset and under new moon conditions. The achieved sifted key rate was $145\text{bit}/s$ with the actual secure key rate being $4.8\text{bits}/s$ with a 4.5% QBER which is sufficient to encrypt transmissions over $1\text{Gbit}/s$. Recently numerous projects are being developed in order to bring QKD satellites into orbit, such as for example the Chinese Micius spacecraft launched in 2016 [11] and the Japanese SOTA laser communication terminal onboard of the microsatellite SOCRATES. The biggest milestone in free space quantum communication comes from the Micius satellite. For the quantum key distribution mission, two ground stations are cooperating with the satellite, one located in Xinglong at 890 m altitude and the other in Nashan at 2028m altitude. Within a duration of 273s , for the QKD data collection, the ground station collected 3,551,136 events corresponding to 1,671,072 bits of sifted keys. The sifted key rate decreased from 12 kbit/s at 645 km to 1 kbit/s at 1200 km, with an increase at lower elevation angles. After randomly shuffling the key, an algorithm is used for error correction. Finally the secure key calculated was of 300,939 bits corresponding to a key rate of 1.1 kbit/s. This experiments show that despite there being still a long way to go regarding QKD, we will be able to practice quantum communications at big distances and securely in a very near future.

2.3 QKD on LEO Satellites

Implementing QKD in space offers a lot of great advantages, being the main reason the big coverage area that otherwise on Earth wouldn't be possible. In the past years a lot of notable satellite QKD initiatives have been realized. In recent years research on satellite QKD has become more appealing with the emergence of small CubeSats which are very small in size and require low power to function.

QUESS: One of the biggest experiments so far is the QUESS payload aboard the Chinese, MICIUS, 631 kg satellite. The objectives of this mission were implementing a series of quantum scientific experiments between the satellite and the ground base station, such as: Quantum key distribution from satellite to ground: Establishing a long range quantum channel between ground and satellite with a high precision tracking and pointing system. Entanglement distribution to two ground stations: Distributing quantum entangled photons from the satellite to two distant ground stations over a distance of more than 1000 km. This mission results ended up with entanglement distribution over 1203 km and BB84 QKD

up to 1200 km with a QBER of 1% and a shifted key of 14 Kbps [11].

SOTA: Another notable mission was the SOTA (small optical transponder), a small payload of about 5.9 kg with a maximum power consumption while operating of 40 W, aboard the SOCRATES satellite (48 kg and 496 x 495 x 485 mm). The main goal of the mission was to successfully verify the ATP (Acquisition, tracking and pointing) system after receiving the uplink beacon and BER measurements of the two transmitting lasers with different characteristics. Laser 1 (Tx1) being transmitted from a 1 cm aperture telescope with a wavelength of 976 nm and a 500 μ rad divergence angle. Laser 4 (Tx4) being transmitted from a 5 cm aperture telescope with a wavelength of 1549 nm with a divergence angle of 223 μ rad. The SOTA lasercom terminal was operated for more than two years. During this time, all the goals of the mission were achieved, including up to 10 Mbit/s downlinks using two different wavelengths and apertures, verification of the coarse and fine tracking of the ground station beacon, space to ground transmission of pseudo-random sequences and images from the camera on board of the payload and experiments with different error coding sequences. Other successful experiment carried out by SOTA was on space QKD where they achieved 100% degree of polarization with a QBER of less than 5 % [12].

QEYSSat: Honeywell Aerospace is a project selected by the Canadian Space Agency to implement the Quantum Encryption and Science Satellite (QEYSSat). This mission has not been held yet but shows promising results. The QEYSSat mission is set to implement both weak coherent pulses (WCP) source and entangled photons source to evaluate the performance of QKD in space. The bigger challenges that are foreseen for this experiment include accurate tracking, acquisition and pointing and suppressing other light sources that affect the single photon exchange over large distances. The main objective will be to create a quantum link between a ground station and a satellite in LEO using polarized photons, and to use this link to exchange encryption keys between different ground users. QEYSSat is designed for quantum photon uplinks to minimize the complexity of the payload aboard the satellite and to be able to use various quantum sources at the ground station. The QEYSSat payload consists of a telescope, the pointing and tracking assembly (QTRAC), quantum receiver, quantum and beacon sources and support electronics. The beacon source from the payload is used to track the ground terminal and similarly a beacon signal from the ground station is used to track the payload QTRAC.

The link budget for this mission consists on the use of a 0.12 m diameter ground station telescope, with static transmitted wavefront error loss assumed to be -0.9 dB. A WCP operating at 400 MHz and entangled photon source operating at 100 MHz were considered for comparative purposes. The accumulation of errors that are introduced when the beam propagates through the turbulent atmosphere results in beam wandering which implies greater losses at long distances and a beam radius of 10 m at 600 km distance. A beacon laser at 1550 nm was used for tracking purposes [13].

SpooQySat: The purpose of the SpooQySat programme is to demonstrate the violation of the CHSH (Clauser Horne Shimony Holt) Bell's inequality with an entangled photon source that is bright enough to transfer photon pairs from satellite-to-ground. The purpose of the payload (SPEQS-2) aboard the cubesat is to demonstrate and design a small system capable of producing pairs of entangled photon pairs in space and able to send them to Earth. The layout of the payload can be seen in the next figure.

The pump laser transmits light at a 405 nm wavelength which is filtered through an optical half-wave

plate (HWP). The light is then sent through two crystals (BBO 1 and 2). The crystals are aligned such that one crystal produces horizontal polarized photons and the other vertical polarized photons. The amount of vertical and horizontal polarized photons is always be the same, since there is a 50 percent chance the light goes through crystal 1 or 2. After passing through the crystals, one photon will have a wavelength of 760 nm and the other a wavelength of 867 nm. The dichroic mirror (DM) is used to dump the extra light that is not transferred into photons. After this the photons are entangled by going through compensation crystals (BBO 3 and 4). This optimises the correlation between the photons, making it possible for the photons to be measured by the use of APD detectors [14].

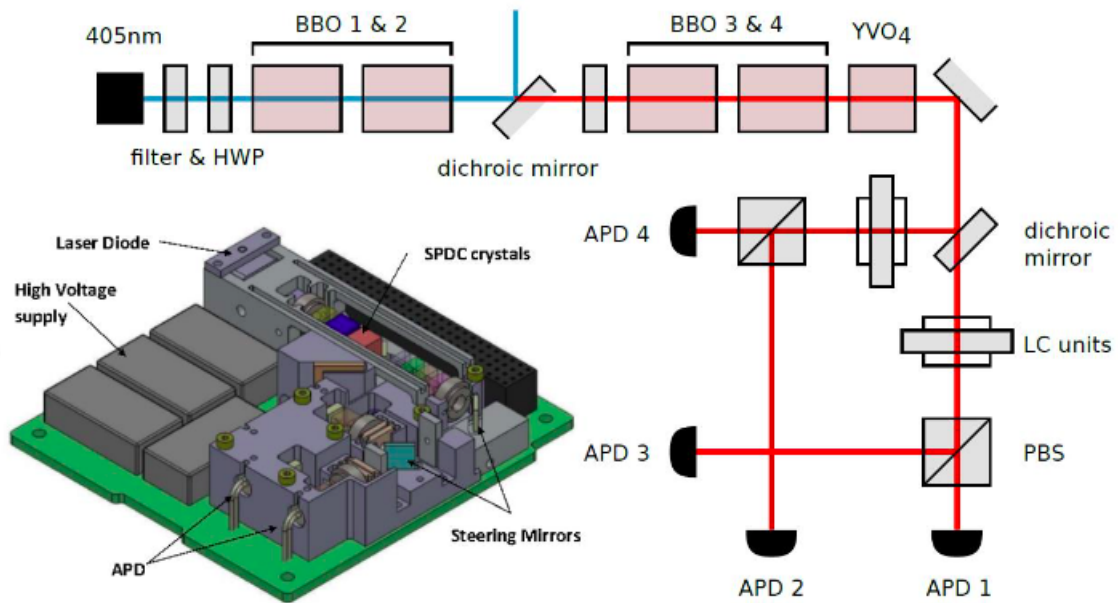


Figure 2.1: Layout of the SPEQS-2 payload [14]

The final payload design occupies 2U in volume and weights around 0.9 Kg. To verify the payload capability for space, the researchers tested it's ability to withstand the great vibration and thermal changes experienced during a a rocket launch and in-space operation. The photon source managed to maintain high quality entanglement throughout the testing and through the temperature oscilation from -10 to 40 C, thus preserving crystal alignment. The payload was incorporated onboard SpooQy-1 on June 17, 2019, successfully generating photon-pairs over temperatures ranging from 16 to 21.5 C [15].

NanoBob: NanoBob is a cubesat concept mission for quantum key distribution in space. NanoBob is set to demonstrate the feasibility of quantum communication in space between a ground station and a nanosatellite in an uplink configuration. By placing the photon source (Alice) in the base station it is possible to reduce the dimensions and the power needed at the satellite. The receiver at the satellite is compatible with multiple QKD protocols. The NanoBob cubessat will be launched into a 550 km altitude orbit and is envisaged to have various encounters with multiple base stations on Earth. A study Size, Weight (mass) and Power (SWaP) analysis by the authors, estimates a volume of 12 U, mass of 9 kg and a peak power consumption of 34 W while operating. The optical module consists of a telescope with high light gathering power capacity, a quantum channel polarization analyzer and a tracking unit

to detect the ground-to-satellite beacon laser. It is complimented with a small diameter telescope that focuses the satellite beacon laser, as well as two corner cubes that retro-reflect the OGS beacon laser. The main telescope maximizes the number of photons gathered by the quantum channel from the base station to the satellite. A Cassegrain telescope was designed with an aperture of 150 mm and with a Field Of View (FOV) of the quantum channel's detectors (100 μm diameter) equal to 215 μrad (45 arcsec, corresponding to a circular footprint of 120 m diameter with the satellite at an orbital height of 550 km). Knowledge of the spectral radiance of the area of the OGS then enables to calculate the expected background count rate. A previous study measured a photon flux of 10^{10} to $2.5 \cdot 10^{11} \text{ s}^{-1} \text{ sr}^{-1} \text{ m}^{-2}$ at the Canary Islands with a spectral band pass filter of 10 nm centered at 810 nm, depending on the moon phase. Resulting in an estimated count rate of less than 400 cps. The background can be further reduced using a narrower bandpass filter. The FOV of the beacon detector is 9 mrad. The compact telescope allows for the entire optics module to be shorter than 200 mm. The polarization detection unit analyzes the photons captured by the light in either one of two bases. The random choice between either the horizontal-vertical (HV) or the diagonal-antidiagonal (DA) basis is made by a 50/50 beam splitter (BS). Following the BS a half-wave plate (HWP) oriented at 22.5° in one of the two paths is used to rotate the polarization direction by 45° . Polarizing beam splitters (PBS) in both paths enable the polarization analysis. The probability of a photon ending up in the wrong path (a vertically polarized photon being detected by the "horizontal detector" instead of the "vertical detector") is not larger than 1%, as such a detection error increases the coincidence error and reduces the signal-to-noise ratio and visibility. Importantly, this error includes the possible misalignment of the OGS and satellite polarization bases. The OGS laser beacon signal is used to improve absolute accuracy and to improve alignment precision to the 10-rad level, beyond what would be possible using the star tracker only. The authors concluded, with this study, that QKD is feasible between an Earth station and a 12U cubesat in an uplink configuration. Also, taking into account the atmospheric conditions at the sight of the experiment and the CubeSat orbit, they expect to generate $2 \cdot 10^7$ secure bits per year with a combined cost of a single satellite to be about 1.5M euros [16].

Fraunhofer quantum satellite: At the Fraunhofer Institute for Applied Optics and Precision Engineering in Jena, a stable, space-suitable source for entangled photons is being developed. The source is based on a hybrid design in which a non-linear, periodically poled crystal (ppKTP) from two sides in the arrangement of a Sagnac interferometer with a max power of 8 mW at 405 nm is pumped. The resulting excited Spontaneous Down Conversion (SPDC) in the crystal generates polarization-entangled photons in the transmitter and receiver channel at a rate of up to 300,000 pairs per second with the visibility of these photon pairs in the range 96-99 %.

For the space-suitable design of the EPS, a compact, precision mechanics, thermo-mechanically stable platform has been selected, on which the optical setup of the source was integrated via effective and deterministic assembly algorithms, achieving high accuracy's. Temperature leveling of the ppKTP crystal within this platform was realized at temperature homogeneity of 0.1 K along the 30 mm long optical axis of the crystal. To fixate the sensitive alignment state of the EPS with respect to long-term stability under space conditions, specific laser based soldering and optics glueing technologies have

been used. The source was positively evaluated for its quantum optical parameters within and after typical test cycles for space assembly for thermal and mechanical loads as well as thermal-vacuum.

2.4 QKD on HAP's

The application of HAPs has been the subject of study worldwide for the past few years. HAPs offer a wide range of advantages over LEO satellites. For example LEO satellites have an orbital velocity of about 7 m/s which makes it difficult to have a continuous link connection for more than a short period of time. Whereas HAP's are quasi stationary and can maintain the connection for several hours if the atmospheric conditions are favourable (ex: non existence of clouds). Other advantages are that HAP's are easy to deploy and are much cheaper than using a satellite. Despite LEO satellites having a larger footprint because of their orbital altitude, with a HAP's network or with base stations diversity the coverage area can be greatly increased. Other advantages are for example, contrary to a satellite the HAP can be brought down for payload repair or reconfiguration. The losses due to beam misalignment also decrease since these losses mainly occur for distances greater than 20 km (altitude of the HAP's) for uplink connections.

HAPs provide a platform for scientific, military, or commercial payloads at heights of 17 to 22 km, which is above civil air routes and clouds, but below orbiting satellites. HAPs with endurance between 12 hours and 1 year may be powered by fuel, regenerative fuel cells, and/or solar energy. Similar to the way satellites are powered, solar power can be used, since they are set in the stratosphere no clouds will block the sunlight.

Using QKD on HAP's is still a recent idea but there already some on going projects being developed. By combining the features of terrestrial and satellite communication systems, HAP-based systems offer a number of benefits:

Wide service coverage: Because of the high altitudes of HAPs the service area that can be covered is significantly larger compared to terrestrial infrastructure, being able to serve areas up to 200 km in diameter depending on the elevation angle of the HAP.

Reduced obstruction: Compared with terrestrial infrastructure, obstruction is not a problem since the elevation angle is flexible.

Environmental advantages: By reducing the need for terrestrial infrastructure and because of the fact that many HAP's can be powered by renewable energies like solar panels.

Rapid deployment: A HAP can be launched within a few hours, much faster than any terrestrial infrastructure with the same coverage or any satellite. This has advantages regarding a fast operational availability, for fast bridging or filling a network gap, or in the case of an emergency or a disaster.

Easy servicing: Contrary to a satellite, HAPs can be brought down for the payload or the vehicle itself to be repaired, upgraded, or reconfigured.

Low cost: In terms of launch costs a HAP is considerably cheaper than a satellite. Especially because a LEO satellite might need much more base stations for the continuous availability of the signal.

Less link losses: Compared to a communication link between a ground station and a satellite, a

scenario involving HAP's suffer from less influence due to atmosphere turbulence or beam misalignment. Since HAP's are situated well above the clouds, a HAP-to-satellite relay communication scenario is well suited for optical free-space communication, leading to a very high communication capacity.

Close range: Because of the intermediate position of a HAP between ground and satellite, the link can be closed more easily. Also the signal delay from a HAP to the ground is negligible compared to satellite-ground links, reducing the propagation delay.

Chapter 3

Theoretical Overview

3.1 Satellite Coverage Area

The satellite coverage area on Earth depends mainly on the orbital parameters such as the satellite position relative to a point on the Earth surface. LEO satellites move at around 7.5m/s relative to a fixed point on the earth surface. Ground stations can communicate with LEO satellites only when there is LOS (Line of sight). The coverage area of a satellite is an elliptical area projected on the Earth surface. The largest coverage area is achieved with 0° elevation, but in order to avoid obstacles i will range the elevation from 2° to 10° . The following equations are based on [17].

The geometry between a satellite and Earth can be seen in figure 3.1. The different points represent the satellite (SAT), the base station (P), the distance between the satellite and the base station (d) which depends on the elevation angle (also called slant range), the line passing through P represents the horizontal plane, T is the point on the surface of the Earth that is collinear with the line that goes from the satellite to the center of the earth. There are four variables that we have to consider: ε_0 (elevation angle), α_0 (nadir angle), β_0 (central angle) and d (slant range). These variables are expressed by the following equations [17]:

$$\varepsilon_0 + \alpha_0 + \beta_0 = 90^\circ \quad (3.1)$$

$$d \cos \varepsilon_0 = r \sin \beta_0 \quad (3.2)$$

$$d \sin \alpha_0 = R_e \sin \beta_0 \quad (3.3)$$

With R_e being the Earth Radius.

The most important parameter will be the slant range (d) which is affected by the elevation angle. From this image and applying geometrical equations we get [17]:

$$r^2 = R_e^2 + d^2 - 2R_e d \cos(90 + \varepsilon_0) \quad (3.4)$$

Which solved in order of d and substituting r by $r = H + R_e$, with H being the distance from the

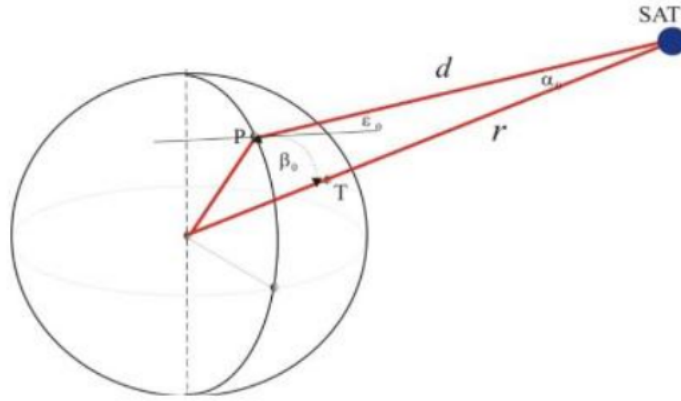


Figure 3.1: Satellite and Ground Station Geometry

satellite to the Earth's surface in the direction of the Earth center when pointing towards the center of the Earth, different from d that is the distance from the satellite to the Earth station we get:

$$d(\varepsilon_0) = R_e \left[\sqrt{\frac{H + R_e^2}{R_e} - \cos^2 \varepsilon_0} - \sin \varepsilon_0 \right] \quad (3.5)$$

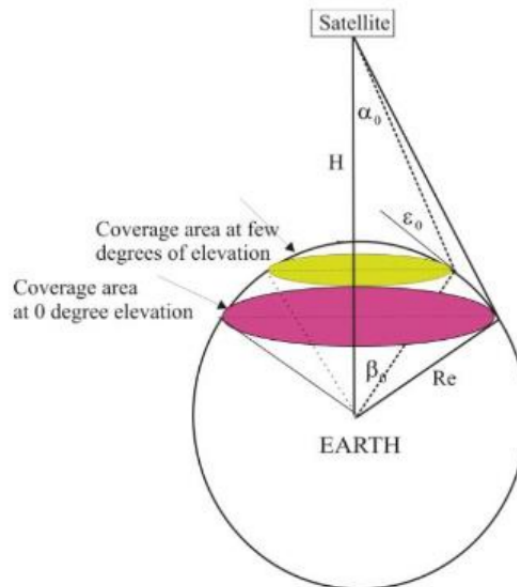


Figure 3.2: Geometry from the coverage point of view

From this image and applying the sinus theorem we get the equation [17]:

$$\sin \alpha_0 = \frac{R_e}{R_e + H} \cos \varepsilon_0 \quad (3.6)$$

For different elevations (ε_0) we calculate α_0 and then based on equation (1) we calculate β_0 . Now knowing these parameters we are able to calculate the surface of the covered area which is described

by the following equation [17]:

$$S_{coverage} = 2\pi R_e^2(1 - \cos \beta_0) \quad (3.7)$$

3.2 Bit-Error Rate

The performance of the optical receiver in a digital transmission system is measured by the Bit-Error Rate (BER). The BER is defined as the ratio between the number of received bits incorrectly detected and the total number of bits transferred in a given time interval. Usually for this kind of optical communications the values vary between 10^{-6} and 10^{-9} [18].

The two mainly types of modulation used in Free-Space optical communications are the OOK (On-Off Keying) modulation and the PPM (Pulse Position) modulation.

BER - OOK Modulation

The OOK modulation consists in a binary technique where each time slot corresponds to one bit. The bit '1' is indicative of the presence of a laser pulse, while bit '0' indicates the absence of signal. The modulation line code can be NRZ (Non-Return to zero) where the pulse duration has the same bit period and RZ (Return to zero) where the pulse has a shorter duration than the bit period. The NRZ pulses are the mostly used due to the fact that they require less bandwidth [18].

For OOK modulation the BER can be calculated by the following expression:

$$BER_{OOK} = \frac{1}{2} \operatorname{erfc} \left(\frac{Q}{\sqrt{2}} \right) \quad (3.8)$$

where Q is the SNR given by:

$$SNR = \frac{V_1 - V_0}{\sigma_1 + \sigma_0} \quad (3.9)$$

V_0 and V_1 are the values of the mean voltage for the logic levels '0' and '1'. σ_0 and σ_1 are the square roots of the noise variances for symbols '0' and '1'.

BER - PPM Modulation

PPM modulation consists in dividing the transmission allocated time of a symbol in M equal time slots (M is the modulation order). To represent a certain symbol, a pulse is sent only in one of the M slots, as shown in the following picture:

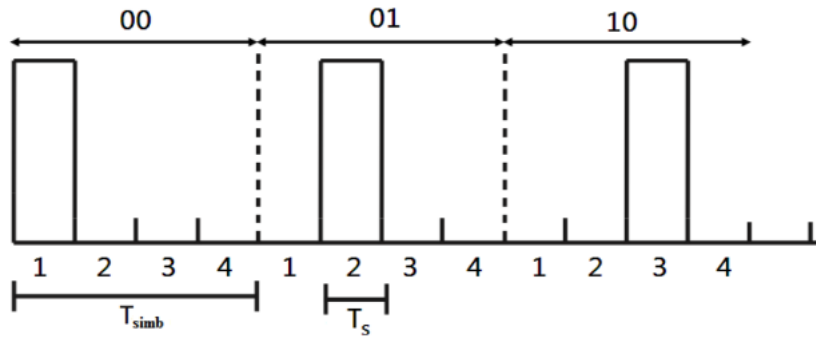


Figure 3.3: 4 - PPM Signal [19]

The number of time slots, M , depends on the bitrate D_b , and is given by:

$$T_{simb} = \frac{k}{D_b} \quad (3.10)$$

And the duration of the slot, T_s is given by:

$$T_s = \frac{T_{simb}}{M} = \frac{k}{M \cdot D_b} \quad (3.11)$$

The following study of the BER for a PPM Modulation using an APD receiver is based on the analysis in [20].

The receiver used for BER analysis is an avalanche photodiode with a trans-impedance amplifier (APD-TIA). For PPM the relationship between the bit error rate and the symbol error rate is given by:

$$BER = \frac{M}{2(M-1)} SER \quad (3.12)$$

The turbulence channel considered for the BER analysis is the additive white Gaussian noise (AWGN) channel. AWGN channel is a good model for satellite and space communication links because it's free from some impairments like multipath, interference, etc. The receiver also contains the AWGN from the transimpedance amplifier (TIA). The author assumes that the light intensity in both the signal present 'ON' and signal absent 'OFF' slot follows a Gaussian distribution. All M slots are independent and have noise as equally distributed Gaussian random variables. With the Gaussian approximation we apply Q-factor analysis (The Q-factor suggests the minimum signal-to-noise ratio (SNR) required to obtain a specific BER for a given signal) to find the SER:

$$SER \leq (M - 1)Q \left(\frac{\mu_1 - \mu_0}{\sqrt{\sigma_1^2 + \sigma_0^2}} \right) \quad (3.13)$$

Where μ_1 and μ_0 are the mean value of signals in 'ON' time and 'OFF' time of the detector:

$$\mu_0 = R.g.(P_0 + P_{bm}) \quad (3.14)$$

$$\mu_1 = R.g.(P_1 + P_{bn}) \quad (3.15)$$

The extinction ratio (ER) of the transmitter should also be considered for BER calculation.

The relationship between the ER, M, P_0 , P_1 and P_{avg} is given by:

$$\frac{P_0}{P_{avg}} = \left[1 - \frac{1}{M} \left(1 - \frac{1}{ER} \right) \right]^{-1} \quad (3.16)$$

$$\frac{P_1}{P_{avg}} = \left[\frac{1}{M} + ER \left(1 - \frac{1}{M} \right) \right]^{-1} \quad (3.17)$$

Where P_0 and P_1 are the optical power received at the detector during 'ON' and 'OFF' time of pulse and P_{avg} is the average power transmitted. ER is the extinction ratio ($\frac{P_0}{P_1}$) of the transmitter and M is the order of the PPM modulation. We conclude that the required Q factor is given by:

$$Q_{req} = \frac{\mu_1 - \mu_0}{\sqrt{\sigma_1^2 + \sigma_0^2}} \quad (3.18)$$

So, the Symbol error rate and the Bit error rate are given by:

$$SER = (M - 1) \cdot \frac{1}{2} \cdot \text{erfc} \left(\frac{Q_{req}}{\sqrt{2}} \right) \quad (3.19)$$

$$BER = \frac{M}{2(M - 1)} SER \quad (3.20)$$

3.3 Photodetectors

The photodetector is the element of the optical receiver used to convert the optical signal into an electrical signal (direct detection - DD receivers employ a photodiode as square-law device, resulting in an electrical signal proportional to the power of the incident signal, i.e. the optical signal power is directly measured. Any optical phase or polarization information is lost). The most commonly used photodetectors in optical communications are the photodiodes because they have the best characteristics, such as small size, high sensitivity and low cost. There are two types of photodiodes used in optical communications, the pin photodiode and the avalanche photodiode (APD).

The APD is constructed to include a very high electric field region called the avalanche region. This region corresponds to the zone where the electric field is greater than the minimum required E_m , to cause the breakdown of the $n^+ - p$ junction and to allow signal amplification [18].

The APD performance is characterized by its responsivity, R_{APD} , which is the relationship between the output electric current and the optical power incident on the APD. The APD responsivity is given by:

$$R_{APD} = \frac{\eta \lambda}{1.24} \quad (3.21)$$

With η being the quantum efficiency of the detector.

An APD multiplies the generated primary photoelectrons by its avalanche gain M (e.g. $M = 100$ for

Si APDs and $M = 10$ for InGaAs APDs). This effect comes at the expense of multiplication noise. The following table presents typical photodetectors characteristics [21].

Table 3.3 - Photodetector Characteristics

Photodetector	Wavelength (nm)	Responsivity (A/W)	Dark Current (nA)
Silicon PIN	550 - 850	0.41 - 0.7	1 - 5
Silicon PIN	850 - 950	0.6 - 0.8	10
InGaAs PIN	1310 - 1550	0.85	0.5 - 1.0
InGaAs APD	1310 - 1550	0.80	30
Germanium	1000 - 1500	0.70	1000

Photodetection Noise

The electrical current generated by the photodetector is directly proportional to the incident optical power. However this current is not always constant and has fluctuations caused by different types of noise such as the quantum noise and the circuit noise [18]. The optical signal that is incident on the photodetector corresponds to a certain average number of photons per unit of time. The time slot between photons is random and the photocurrent generated by the photodiode is not a continuous process. The photodetector generates a small current in the absence of any optical signal. This current is called dark current, I_d , and comes from the thermally generated electron-hole pairs. This dark current also affects the quantum noise at the photodiode [18].

The quantum noise, in certain situations called shot noise, is the random fluctuations in the number of photons that reach the detector from point to point, and is given by:

$$\sigma_q^2 = 2q(r_0 P_i + I_d) M^2 M^x B_{e,n} \quad (3.22)$$

Where q is the electron charge, M is the avalanche gain, x is a photodiode material parameter with values between "0" and "1" and $B_{e,n}$ is the equivalent noise bandwidth from the optical receiver.

The circuit noise depends on the temperature and resistive and active elements in the optical receiver, so its value depends on the remaining electrical elements present in the receiver, such as the amplifier.

Usually the output signal of the photodetector is very weak and needs to be amplified in order for it to be processed by the other system devices. So an electrical amplifier is used to amplify the electrical current generated by the photodetector. As mentioned before, the electrical components of the photodetector contribute to the circuit noise.

The circuit noise current variance is given by:

$$\sigma_c^2 = \left[\sqrt{\frac{4k_B T F_n}{R_L}} \right]^2 B_{e,n} G_A^2 \quad (3.23)$$

Where G_A is the amplifier gain, k_B is the Boltzmann constant, T is the absolute temperature R_L the load resistance of the photodetector and F_n is the noise factor of the amplifier.

The total noise current variance, σ_n^2 , is the sum of the quantum and circuit noise variances:

$$\sigma_n^2 = \sigma_q^2 + \sigma_c^2 \quad (3.24)$$

3.4 Pointing System

Free-Space Optics offer many advantages for systems with limitations regarding size, weight and power. To achieve this potential, one of the main limitations for LEO satellites concerning FSO communications has to do with the PAT (pointing, acquisition and tracking) system that must be very accurate since the satellite has a certain velocity and it must have the laser constantly pointing to the base station. On the other hand for HAP's, one important thing to take into consideration is that the BS is stationary and the HAP's itself is quasi-stationary so the establishment, measurement and maintenance of the links is much less demanding compared to a LEO satellite, since beam tracking and adjusting are less necessary [22].

Despite the tracking on HAPS being much more easier than on LEO satellites, there is still the need for a tracking system that complies with the movement of the spacecraft. This chapter will be based on NODE (Nanosatellite optical downlink experiment), which is a low-cost, commercial off the shelf (COTS) laser downlink experiment, being designed and developed at MIT [23]. NODE is approximately 1U and so is a communications payload easily applicable to numerous CubeSat's. It was envisioned to be able to have at least a 10 Mbps data rate but is designed to be scalable so that much higher rates can be achieved in the future. The 1550 nm wavelength was chosen because its wide usage in the optical area means a wide availability of COTS components. The NODE design also has an uplink beacon laser that is transmitted from the optical ground station (OGS) and is used to facilitate tracking. This uplink laser is detected on the CubeSat, who then has accurate knowledge of where the BS is, and then uses a FSM (Flexible steering mirror) to track it [23]. Node uses different wavelength lasers for different purposes:

- The beacon signal is a 976 nm laser used to detect the base station.
- The downlink signal is a 1550 nm laser used to transmit data.

- The 635 nm laser is used as a feedback laser for the FSM pointing angle.

Optical Hardware

In this section is given a brief description, based on the author description, about all the optical components that are used on the NODE experiment. It will focus mainly on the pointing system and is based on the description given by [23].

The NODE generates two optical signals, the downlink signal which is a 1550 nm optical signal used for the transmission and an uplink signal (beacon laser) which is just used for calibration purposes. Due to the significant losses in free space optical communications, the beacon camera is prepared to detect a very low power laser. The laser used is a 1 mW fiber coupled 635 nm laser diode manufactured by QPhotonics [23].

For the laser uplink tracking, the most important piece of hardware is the on-board camera at the nanosatellite. The choice of the wavelength for the beacon laser, near IR (InfraRed), allows for the use of silicon detectors which are much more cheaper than the ones used at the IR spectrum, like the InGaAs APD. A compact COTS camera was selected from the German manufacturer Matrix vision. This camera incorporates the Aptina MT9P031 FPA, which has a small pixel size. The small pixel size allows for using shorter focal length lenses, therefore reducing space while obtaining good angular resolution crucial for beacon tracking. This sensor has a quantum efficiency of 3% at 967 nm [23].

The focusing lens is used to detect the incidence of the beacon laser on the detector and then determine the angle of the incident beam. The most important thing when choosing a lens is the Focal Length, which determines the field of view of the detector. Also the larger the lens aperture, the more photons are detected and therefore increasing the gain at the receiver. The lens chosen for NODE is the Xenoplan 1.4/23 by Schneider Optics. This lens has a focal length of 22 - 5 mm and an aperture size of about 16 mm [23].

This mirror is used to determine the route of the optical signal depending on the wavelength. Acts as a mirror for the 1550 nm signal (downlink) since it reflects the signal out of the main satellite aperture. Acts as a beamsplitter, partially passing and partially reflecting the beacon laser to be detected on the camera lens. Acts as a window for the 976 nm signal so that the beacon detect-ability is not worsened. For this mirror, the DMLP1800R rectangular longpass dichroic mirror from Thorlabs was chosen. The tests showed that with this mirror the 1550 nm signal has a 99% reflection rate, it reflects 85% of the 635 nm light towards the camera after reflection from the side mirror and the other 15% passes through. Taking into account the losses on the dichroic and regular mirror, at least 10% of the power from the calibration laser gets through to the lens, which is more than enough [23].

The bandpass filter is added to the satellite main aperture to block light from earth and therefore minimize the noise on the beacon detector. A double band pass filter was chosen to attenuate all wavelengths except the downlink 1550 nm wavelength and the 976nm beacon wavelength. There weren't any COTS readily available solutions on the market so a custom filter was ordered from Omega Optical. This

filter has a transmission efficiency of about 85% for the desired wavelengths with a pass-band bandwidth of 80 nm for the 1550 nm and 40 nm for the 976 nm. Out of this band has a transmission of 0.02% which results in -37dB attenuation [23].

The FSM (flexible steering mirror) is crucial to the pointing system as it guides the downlink beam in the direction of the ground station based on the beacon's angle of incidence. For the NODE it's used a MEM FSM (microelectromechanical flexible steering mirror) manufactured by Mirrorcle Technologies, with a mirror diameter of 3.6 mm and a steering range of 3 degrees.

A collimator is a device which narrows a beam of particles or waves. Turns the optical signal propagated in the fiber into a free space beam. The collimator used on the NODE is the CFS5-1550-APC from Thorlabs. With a FWHM divergence angle of 1.3 mrad, it is calibrated for the intended wavelength of 1550 nm, has 1mm diameter and 2mm in length [23].

To be able to have both the downlink and the uplink (calibration signal) signals going to the FSM, a coupler is needed to couple both signals into the same fiber and fed to the same collimator. For this a Wavelength-division multiplexer by Thorlabs was chosen, so that it can combine both 1550 nm and 980 nm signals into the same fiber [23].

In the following picture drawn by the author in [23] , we can see how the tracking and pointing system works in the NODE experiment. The uplink beacon signal is sent from the base station and detected by an on board camera at the satellite, the signal being transmitted (downlink) in red is amplified in an optical fiber, to ensure that the downlink signal and the calibration signal share the same exact beam path to the FSM, they need to be coupled into one fiber and fed into the same collimator, and then go to the FSM where it is reflected by steering the mirror based on the angle of incidence of the beacon laser.

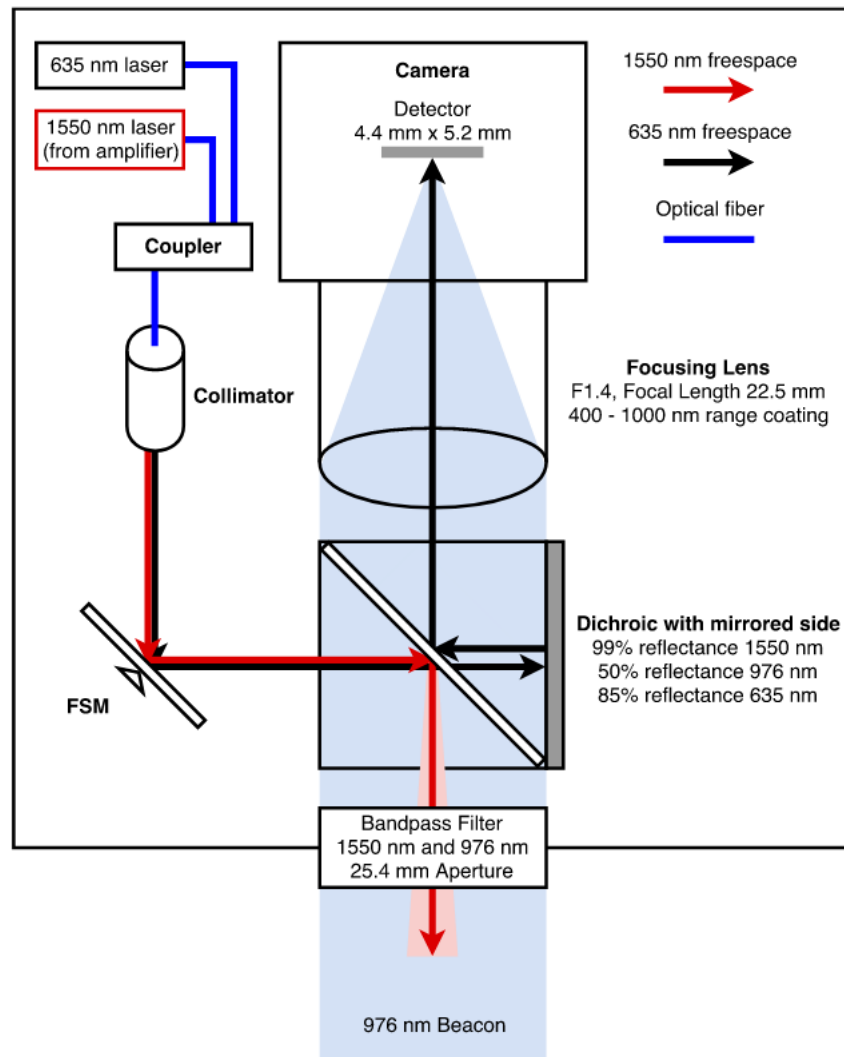


Figure 3.4: Diagram of the NODE pointing and tracking system [23]

3.5 Link Budget Analysis

Free space optical communication links transfer information between a transmitter and a receiver using an optical carrier and a free space channel. During this transfer there are many aspects that affect the signal such as the atmospheric effects. For FSO communication, eddies in the turbulent atmospheric channel cause random variations in the intensity of the received signal. Atmospheric turbulence, the main attenuation parameter in Earth to satellite FSO, is the atmosphere temperature and pressure variations resulting in fluctuations in the atmospheric density, affecting the signal received. The issues involved in the FSO communication in laser uplink are different from the ones in the downlink for LEO satellites. For HAPs since the altitude is around 20 km the effects of the turbulence on the downlink and uplink are similar, with the PAT being the main issue. For LEO satellites in the case of laser uplink (ground to satellite), the beam comes immediately in contact with the atmosphere and therefore suffers more from distortion and pointing instability due to changes in the refractive index of the atmosphere. On the other hand, for laser downlink (satellite to ground), it causes the beam to spread geometrically

(caused by beam divergence loss), and very little spread is due to the atmospheric effects. Due to these aspects, the effect of atmospheric turbulence is smaller on the downlink propagation compared to the uplink propagation, as the beam goes through a non-atmospheric path until it reaches about 30 km from the Earth's surface.

Quantum Key Distribution systems rely on optical communications link analysis to have enough photons arriving at the receiver. The main factors that have to be taken into consideration regarding optical communications are the distance between the transmitter and the receiver, the operating wavelength, all the losses related to the atmospheric conditions, geometrical losses, the channel turbulence, the background noise and the optical losses.

In the following study we will take a look at the different parameters that affect the channel loss on an optical link based on Pfennigbauer et al. method [24] and based on the paper by [1], where two different methods to calculate the channel losses are used and compared.

Geometrical Losses

These losses result from the natural spreading of the beam and make the beam deviate from its original path. They are given by:

$$L_{geo} = 20 \log_{10} \left(\frac{D_{tx} + \frac{H_{hap}}{\sin \alpha} 1.22 \frac{\lambda}{D_{tx}}}{D_{rx}} \right) \quad (3.25)$$

Where D_{tx} is the transmitter aperture size, D_{rx} is the receiver aperture size, R_{Los} is the line of sight distance, H_{hap} is the altitude of the HAP, α is the elevation angle and θ is the beam divergence angle.

Attenuation due to fog, snow and rain

This type of attenuation has to do with the visibility range of the Link. The visibility range for different weather conditions such as fog, snow and rain, according to Kim model is given by:

$$L_{fog} = \frac{3.91}{V} \left(\frac{\lambda}{550} \right)^{-p} (dB/km) \quad (3.26)$$

$$L_{snow} = \frac{58}{V} (dB/km) \quad (3.27)$$

$$L_{rain} = \frac{2.8}{V} (dB/km) \quad (3.28)$$

where

$$p = 1.6 \text{ when } V > 50$$

$$p = 1.3 \text{ when } 6 < V < 50$$

$$p = 0.36V + 0.34 \text{ when } V < 6$$

Where V is the visibility range (km) and p is the size distribution coefficient of scattering.

The distance that the optical signal travels through weather is given by:

$$R_w = \frac{H_w}{\sin \alpha} \quad (3.29)$$

Attenuation due to the misalignment of the beam

Misalignment can occur due to the turbulence in the atmosphere, which is the constant difference in temperature and pressure along the stratosphere. This difference can cause random deflections in the beam with its centroid being randomly displaced:

$$L_{p1} = 0.54R_{Los}^2 \left(\frac{\lambda}{D_{tx}} \right) \left(\frac{D_{tx}}{r0} \right)^{\frac{5}{3}} \quad (3.30)$$

The random movements of HAPs due to, for example, wind can cause difficulties in the pointing system, which result in attenuation given by:

$$L_{p2} = \exp\left(\frac{-8\theta_j^2}{\theta^2}\right) \quad (3.31)$$

Link Budget from NanoBob

To make a comparison between some results, the author makes a comparison between different methods used to calculate the link budget. The other method is based on [16]. This method is described as:

$$L_{Nano} = \frac{L^2(\theta_T^2 + \theta_{atm}^2)}{D_R^2} \frac{1}{T_t(1 - L_p)T_R} 10^{\frac{A_{atm}}{10}} \quad (3.32)$$

Where T_R and T_T are the transmission factors of the receiver and transmitter telescopes, respectively. L_p is the pointing loss due to misalignment, and A_{atm} is the atmospheric attenuation due to Rayleigh scattering and absorption (in dB). It equals to 3 dB at 808 nm and 2 dB at 1550 nm. The beam divergence angle is given by:

$$\theta = 2.44 \frac{\lambda}{D_{tx}} \quad (3.33)$$

And the atmosphere turbulence included divergence angle is given by:

$$\theta_{atm} = 2.1 \frac{\lambda}{r_0} \quad (3.34)$$

According to the author, the definition of θ is different from the one from Pfennigbauer et al. [24] because they don't want to underestimate the effect of atmospheric turbulence so $L \cdot \theta_T$ corresponds to the full diameter of the central spot in the Airy diffraction pattern instead of its radius. And for the same reason the author used the original definition for eq. 3.34, despite some authors using $\theta_{atm} = \frac{\lambda}{r_0}$, without the 2.1 factor, which equals the ratio of the spatial coherence radius to the Fried parameter.

The Fried parameter, r_0 is dependent on the turbulence strength and is given by:

$$r_0 = [0.423k^2 \int_0^h C_n^2(z') dz']^{-\frac{3}{5}} \quad (3.35)$$

To calculate the turbulence strength we can use the Hufnagel-Valley Boundary (HVB) model which is commonly used for ground to satellite communication link. This model includes parameters for the atmosphere up to a height of 24km, can be used for both day and night time and can be used at different locations since it accounts for the variations in wind velocity and on different ground turbulence conditions.

$$C_n^2(h) = 0.00594 \left(\frac{V}{27}\right)^2 (10^{-5}h)^{10} \exp\left(-\frac{h}{1000}\right) + 2.7 \cdot 10^{-16} \exp\left(-\frac{h}{1500}\right) + A \exp\left(-\frac{h}{100}\right) \quad (3.36)$$

Usually the Fried Parameter (r_0) has a typical value of 10 cm to 20 cm at an optical wavelength of 500 nm. The Fried Parameter gets smaller when the turbulence is stronger and theoretically r_0 is proportional with $\lambda^{\frac{6}{5}}$. It's safe to use values around 20 cm for these experiments.

3.6 Optical Payload

The optical payload system layout is based on the Cubesat Infrared Crosslink mission (CLICK) which is a collaboration between the MIT, the Radiation Laboratory (STAR Lab), the Precision Space Systems Laboratory at the University of Florida and NASA Ames Research Center. This experiment aims to develop a pair of CubeSats to demonstrate a nanosatellite inter-satellite link as well as a downlink to a MIT portable optical ground station. On my study we will focus on some of the optical components used in the payload and on the CubeSat to ground Link, with some variations of the parameters used as well as different sizes for the ground station antenna aperture based on a High Precision FOXTECH SEEKER-30 TIR 30X Optical Zoom and Thermal Camera with 3-axis Gimbal [25].

The payload optical system layout is about 1.5U and is shown in Fig. 3.5. There are three optical paths which are the Beacon received signal to aid on the pointing accuracy, and the communications transmitted and received signals. The objective of the fine pointing system (FPS) is to align the transmitted and received communication signals in order to accomplish the pointing requirement. The laser spot sensor is a Quadcell which consists on 4 PIN photodiode sensors. The beacon signal is detected on the quadcell and the output signals are amplified via an APD transimpedance amplifier and a bandpass filter [25].

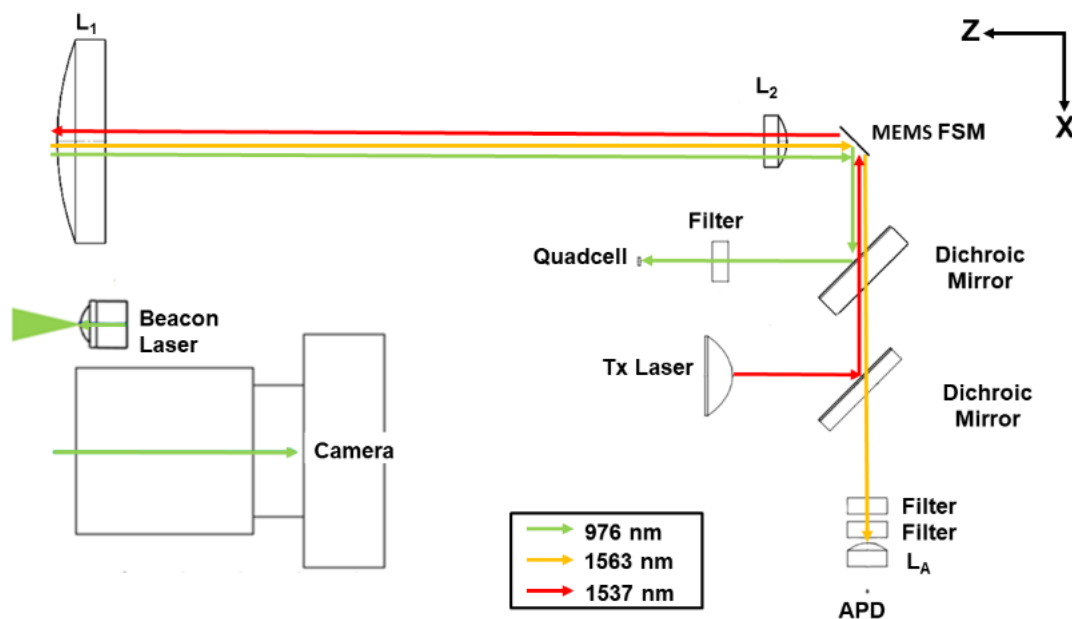


Figure 3.5: CLICK Payload Optical Layout [25]

In order to meet the low SWAP requirements of a CubeSat, the CLICK payload does not use a coarse pointing gimbal, instead relies on the ADCS of the spacecraft. On my study, the payload will be set on a HAP which is capable of higher SWAP requirements. In this type of design the optical bench includes the fine pointing and tracking system and the gimbal will be used for coarse pointing, acquisition and tracking. The gimbal used for the experiment will be the FOXTECH SEEKER-30 TIR 30X Optical Zoom and Thermal Camera with 3-axis Gimbal depicted in Fig. 3.6.



Figure 3.6: FOXTECH Gimbal for coarse pointing, acquisition and tracking

The specifications of the gimbal are in the next table:

Specifications	Values	
Weight (Kg)	1.4	
Working Voltage (V)	4 - 6	
Size (mm)	164.5 127.6 173.5	
Working Temperature (°)	-20° C - +80° C	
Static Current (mA)	400 @ 16V	
Dynamic Current (mA)	500 @ 16V	
Range of control angle	Pitch	+90°
	Roll	+85°
	Yaw	+170°
Control Precision	Pitch and Roll	+/- 0.01°
	Yaw	+/- 0.01°

This 1.5U volume limit payload (96 × 96 × 147 mm) with a mass of 1,5kg can be accommodated in different ways. The selected design layout is shown in figure 3.7.

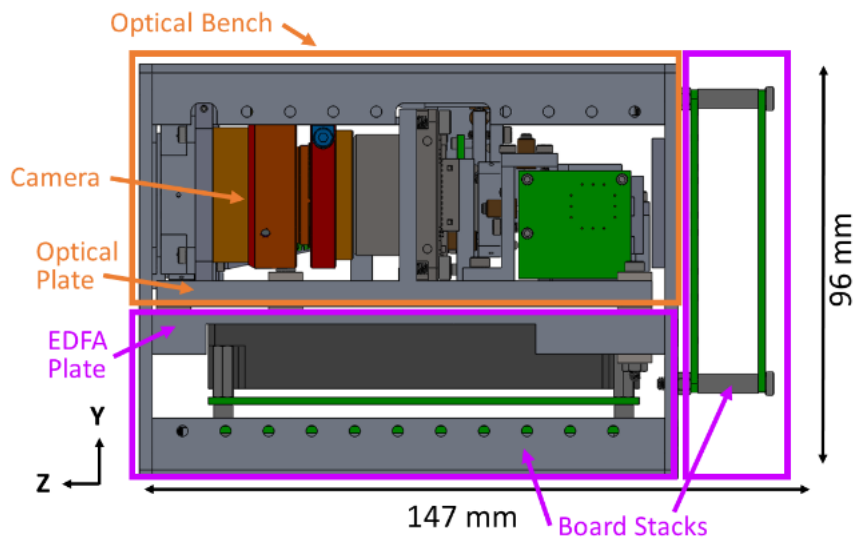


Figure 3.7: Side view of the Payload (+X) [25]

The optical telescope and camera are pointing out of the +Z face. The optical components are coupled into a small volume of $95 \times 56 \times 119$ mm). The upview of the optical components are depicted in figure 3.8.

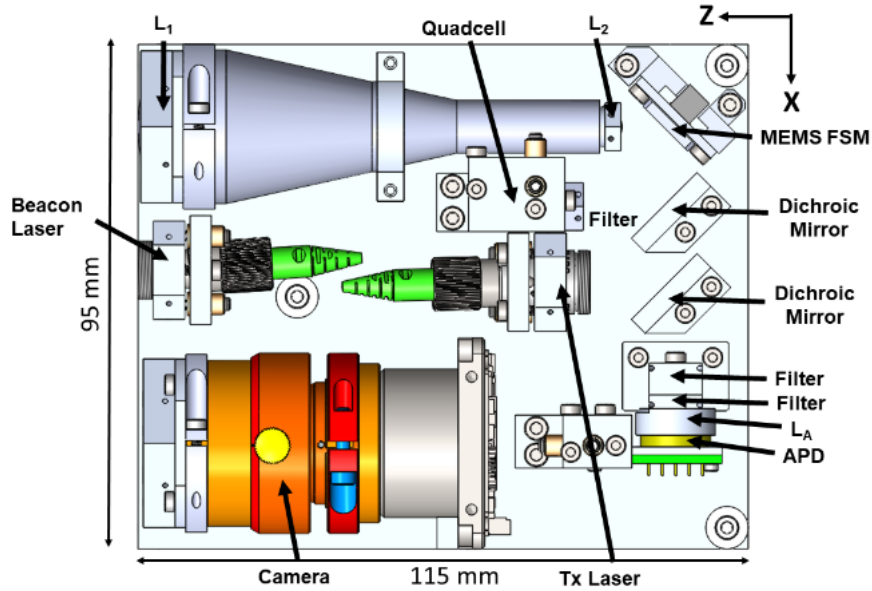


Figure 3.8: Up view of the optical components [25]

Abbreviation	Optical Component Name	Kinematic Mount Req.?
L1	Telescope Primary	No
L2	Telescope Secondary	No
FSM	Fast Steering Mirror	No
D1	1st Dichroic (Quadcell)	No
Filt	Filter	No
Quad	Quadcell	Yes
D2	2nd Dichroic (Tx. Laser)	No
Tx. Laser	Transmitting Collimator	Yes
La	APD Focusing Lens	No
APD	Avalanche Photodiode	Yes
Bcn. Laser	Beacon Collimator	Yes
Camera	Camera	No

Figure 3.9: Optical Components [25]

The APD being used is the RIP1-NJAF APD with a sensor housing diameter of 15.25mm. The following table lists the Camera, telescope and quadcell used in this payload.

Assembly	Optical Component(s)	Component Mass(g)
Camera	Xenoplan 1.4/23-0902 and Filter	94.0 and 2.72
Telescope	Thorlabs A375-C and ASL10142	8.0 and 0.1
Quadcell	First Sensor QP1-6 TO	3.95

The camera used in this payload is the Xenoplan 1.4/23-0902 from Sensorylabs, it features high resolution optics, highest optical imaging performance even with smallest pixel sizes, broadband coating (400 - 1000 nm), compact and low weight, vibration insensitivity for stable imaging performance and focus and iris setting lockable. The technical specifications are presented in the following table:

Technical Specifications	
F-number	1.4
Focal Length (mm)	22.5
Image circle (mm)	11
Transmission window (nm)	400 - 1000
Interface	C-Mount
Weight	94 g
Filter tread	M30.5 x 0.5
Code no.	1001917

For the Telescope lens being used, it has been chosen the Thorlabs A375-C and ASL10142. The A375-C is an aspheric Optical Lense with wavelength range from 1050 to 1620 nm, a focal length of 7.50 mm and a diameter of 6.51 mm. The ASL10142 from Thorlabs in an aspherical optical lense with a focal length of 79.0 mm and a diameter of 2.54 cm. The Quadcell being used is the QP1-6 TO from fist sensor, it features a 1 mm² Quadrant PIN detector, high sensitivity, a small gap and low dark current. Can be described as a Low dark current circular active area quadrant PIN photodiode with a 4 x 0.25 mm² active area. Metal can type hermetic TO52 package with clear glass window. For the dichroic mirror, the DMLP1800R rectangular longpass dichroic mirror from Thorlabs was the one chosen for the NODE satellite mission. On this mission the tests showed that with this mirror the 1550 nm signal has a 99% reflection rate, reflects 85% of the 635 nm light towards the camera after reflection from the mirror and the other 15% passes through. The FSM guides the downlink beam in the direction of the ground station based on the beacon's angle of incidence. For the NODE it's used the A7B1.1

MEM FSM (microelectromechanical fast steering mirror) manufactured by Mirrorcle Technologies, with a mirror diameter of 3.6 mm and a steering range of 3° [25].

3.7 QKD

BB84 Protocol

The BB84 Protocol is a QKD protocol proposed in 1984 by Bennet and Brassard. The objective of this protocol is to encode every bit of the secret key into the polarization state of a single photon. An attempt to measure an incoming photon in an unknown polarization state will introduce disturbance and therefore it will be possible to detect an outside attack. In the BB84 protocol, Alice sends a sequence of pulses where, ideally, each pulse contains a single photon with a certain polarization. Here, Alice sends single photons randomly polarized horizontally or vertically (straight base), or $+45^\circ$ or -45° (diagonal base) where The 'D' polarization corresponds to 1 and the 'A' polarization to 0.

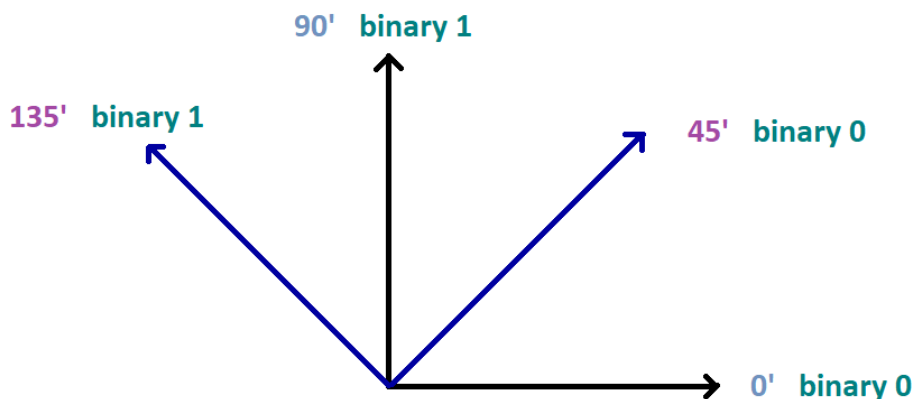


Figure 3.10: Photons Polarized in 2 basis

At the receiver Bob measures the polarization state of the photons with the adequate setup, and he is able to distinguish between the H and V polarizations if he uses the HV basis. In Half of the cases Bob randomly changes his measuring basis to AD. After a certain number of bits have been transmitted, Bob announces which basis he used for each bit and compares it with Alice. Alice then says in which cases they used the same basis and they throw out the bits where they used different bases. After this procedure, called key shifting, they reduce the length of the key twice, and what is left, despite being random, coincides for Alice and Bob. After this procedure they take out a small part of the key, for example 10% and compare it to check for eavesdropping. This part of the key is made public and is later discarded. But if they see that there are errors in the key, the whole key is discarded and the procedure is repeated again [26].

E91 Protocol

The E91 Protocol was proposed in 1991 by Artur Ekert and uses entangled pairs of photons. These can be created by Alice, Bob or by some source separate from them, including the eavesdropper Eve. The photons are distributed so that Alice and Bob end up with one photon from each pair. This scheme relies on two properties of entanglement. First, the entangled states are perfectly correlated in the sense that if Alice and Bob both measure whether their particles have vertical or horizontal polarizations, they always get the same answer with 100% probability. The same is true if they both measure any other pair of complementary (orthogonal) polarizations. This needs for the two distant parties to have exact directionality synchronization. However, the particular results are completely random. It is impossible for Alice to predict if she (and thus Bob) will get vertical polarization or horizontal polarization. Second, any attempt at eavesdropping by Eve destroys these correlations in a way that Alice and Bob can detect [26].

B92 Protocol

The B92 protocol was proposed in 1992 by Bennet and uses two non-orthogonal states, for instance H for 0 and D for 1 (Figure 3.11).

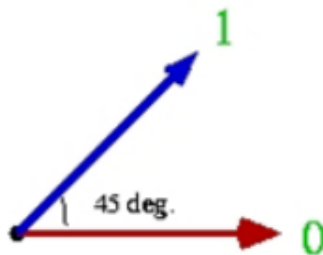


Figure 3.11: Two non orthogonal states, H for 0, D for 1

Alice sends 0's in the HV basis and 1's in the AD basis. Bob chooses the basis randomly, if he gets V polarization in the HV basis, it means it can't be H so he writes down '1'. But if , on this basis he gets a H, it can also be a D, so the result is inconclusive and this bit is discarded (Figure 3.12).

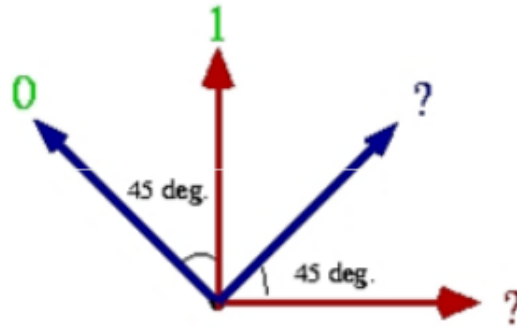


Figure 3.12: Possible results for Bob

The same if Bob uses the DA basis and obtains D, it could be D but could also be H, so the result is again inconclusive. Only if Bob gets an A in the AD basis he writes '0' because it could not be D. The B92 can also be applied to continuous-variable states but is believed to be less secure than the BB84 protocol [26].

QKD Payload

Quantum Key Distribution systems rely on the distribution of either single or entangled photon states. Nowadays the best sources for generating photon states are based on SPDC (Spontaneous Parametric Down Conversion) where they can serve as a pair-source for entangled photon pairs or as a single photon source when one of the photons of the pair is used to indicate the presence of the other. Single photons can also be realized using attenuated laser pulses, where on average, each pulse contains one photon. It is necessary to have a classical communication channel in parallel with the quantum channel in order to establish real-time data post processing (temporal correlation between photons of entangled pairs and between the emission and detection time of single photons).

There are two main types of satellite based quantum key distribution. The first is the untrusted node which assures secure quantum communication between two ground stations via Bell tests, without the satellite taking any part in the security of the communication. This type of QKD requires simultaneous links between the satellite and the two ground stations which is hardly achievable with high key rates. In the trusted node the satellite works as a receiver or as a transmitter.

In this section a brief description of a QKD payload and its subsystems will be given based on the QUARC (Quantum Research Cubesat), a mission to launch 15 low cost 6U CubeSats across the UK [27].

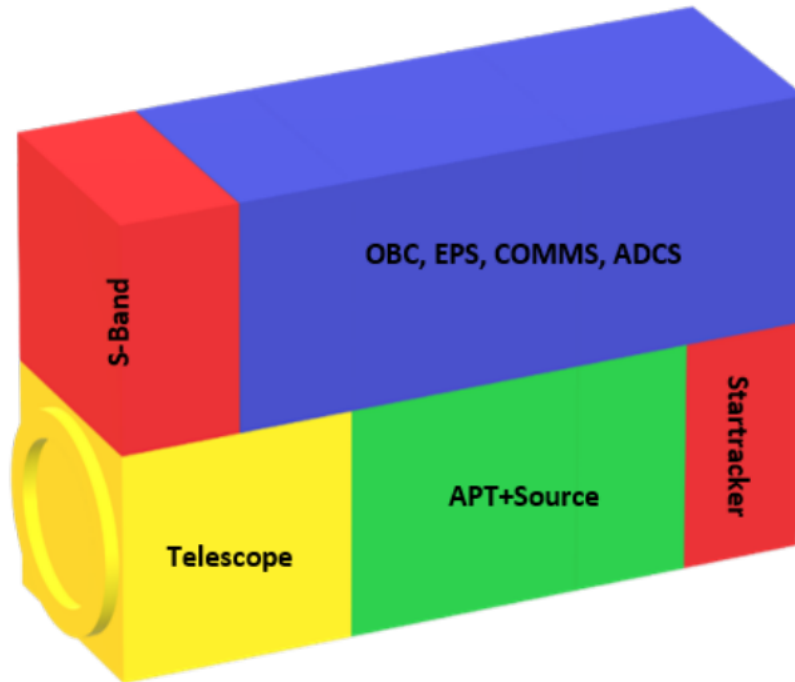


Figure 3.13: Layout of the 6U CubeSat used in the QUARC experiment and its different compartments [27]

In figure 3.13 is depicted the architecture of the 6U payload used on the QUARC experiment. It is divided into 5 different areas, where the biggest one which occupies approximately 3U is reserved for the electrical power system (EPS), the communications (COMMS), the on-board computer (OBC) and the attitude determination and control system (ADCS) which includes and star tracker used to provide sub- 0.25° coarse pointing. The other areas consist of the transmission telescope which occupy 1U, the acquisition, tracking and pointing (ATP) system occupy 1.5U and the payload electronics around 0.5U. An S-band antenna is used to allow high speed radio frequency (RF) communications for the data post-processing. Summarizing, the 6U CubeSat proposed for the QUARC mission, uses 2U of volume for the supporting platform systems, 2U of volume for the telescope system and 2U of volume for the ATP [27].

Photon Sources

A variety of techniques have been proposed for QKD. QKD protocols can be divided into two categories: discrete variable QKD (DV-QKD) or continuous variable QKD (CV-QKD). In DV-QKD information is encoded onto discrete degrees of freedom of optical signals. In CV-QKD, information is encoded into the quadratures of randomly selected coherent states and measured using homodyne or heterodyne detection.

For DV-QKD, there are two main photon sources: weak coherent pulses (WCP) or polarization-entangled photon-pairs. Short attenuated pulses from laser diodes provide controlled weak coherent pulses that are needed to provide photon states for DV-QKD to enhance the security of these systems. Still, each pulse has a finite probability of containing more than a single photon. To avoid eavesdropping, decoy states have been created to reduce the likelihood of photon-number splitting attacks. One party

randomly chooses between two intensities of coherent state signals, which is revealed to the other party, improving the tolerance to losses compared to the BB84 protocol that does not employ decoy states. This helps improving the transmitting distance and the key generation rate. Four laser diodes in a single transmitter are used to address the need for active polarization manipulation, allowing each laser to be identified with a single polarization state. By using a single laser diode coupled to four waveguides, the access to potential eavesdroppers is closed. Each waveguide is capable of a certain amount of polarization rotation and signals are then recombined into a single mode output with four possible polarization states.

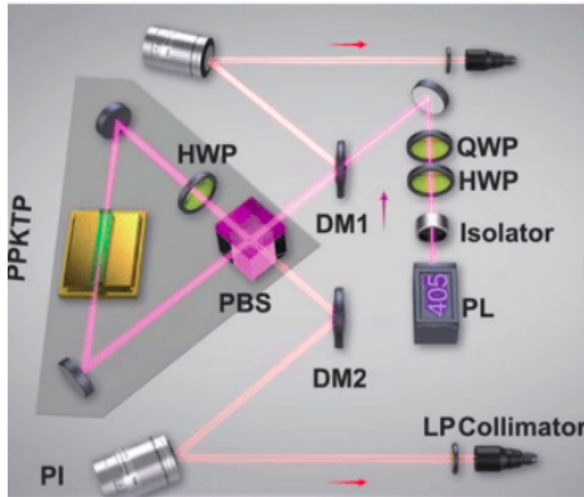
Entanglement-based QKD require the generation of photons using polarization entangled photon pair sources. These sources are based on bulk-crystal, collinear, spontaneous parametric down conversion (SPDC), either periodically-poled potassium titanyl phosphate (PPKTP) or single domain crystals such as beta barium oxide (BBO). SPDC is a non-linear process where a photon spontaneously splits into two other photon of lower energies. The pair of photons are then distributed through a free space link to both Alice and Bob [28].

In order to assess the best QKD terminal for space, a trade-off between both sources has to be performed, taking into account certain aspects such as:

Quantum communication terminal physical features which assess the SwaP (size, weight and power consumption), the terminal performance based on the requirements to perform at a certain link distance, the capability to achieve the expected results, allow quantum link experiments that have a potential for commercial interest and provide a classical optical communication link between the terminal and the base station. Other issues such as the development and the terminal costs, and the growth potential considering the improvement of possible applications such as to grow in link capacity are also of relevance.

Taking into account these aspects, in general, the EPS terminal is larger and heavier than the SPS terminal and also consumes more power. However, the range of possible experiments and their scientific impact is much higher using an EPS terminal than using a SPS terminal.

Entanglement-based secure QKD has been achieved over a physical distance of 1120 km at the Micius satellite experiments between two cities in China. Both ground stations were equipped with a 1.2 m diameter telescope. The satellite is equipped with a entanglement photon source that weights 23.8 Kg. A KTiOPO crystal inside a Sagnac interferometer is pumped by a continuous wave laser with a wavelength centered at 405 nm and a linewidth of 160 MHz, and generates polarization entangled photon pairs at 810 nm. The entangled photons are then guided by two single mode fibers to two transmitters which have a near-diffraction-limited far-field divergence of about $10 \mu\text{rad}$. With a pump power of 30 mW the source is able to distribute up to $5.9 \cdot 10^6$ entangled photon pairs per second. The photons are then sent to two optical ground stations [11]. In figure 3.14 we can see the scheme of the entangled photon pair-source used in the Micius satellite experiments.



PL: Pump Laser
HWP: Half Wave Plate
QWP: Quarter Wave Plate
DM1/2: Dichroic Mirrors
PBS: Polarizing Beam Splitter
PPKTP: Periodically Poled
Potassium Titanyl Phosphate
PI: Piezo steering mirror
LP: long pass filter

*Receivers/analysers are
not shown*

Figure 3.14: A polarization entangled photon pair-source using PPKTP in a Sagnac loop arrangement. Used by the Micius Satellite double-downlink demonstrations [11]

Chapter 4

Results

4.1 Coverage Area

As studied in chapter 2.4 the two parameters that affect the satellite and HAP footprint on Earth are the height at which they are orbiting and the elevation angle which is the angle of the satellite/HAP in relation to the horizon. The smaller the elevation angle, the bigger is the area covered on Earth but the distance traveled is also longer which means that the signal will be more affected by the turbulence and other characteristics that will make the signal received at the detector have bigger losses. Also the elevation angle can not be too small because it will be affected by building when arriving at the Earth surface. In order to achieve the best relation between attenuation and covered area a good choice of the elevation angle is necessary. In the figures 4.1 and 4.2 we see different coverage areas (maximum distance between two points on the Earth surface) for a satellite at 500 km altitude but for different elevation angles. This model characterizes the distance covered with a model that addresses the area on the Earth surface as being a circle which is not entirely correct since the shape of the area varies and is not a circle because of the Earth curvature.

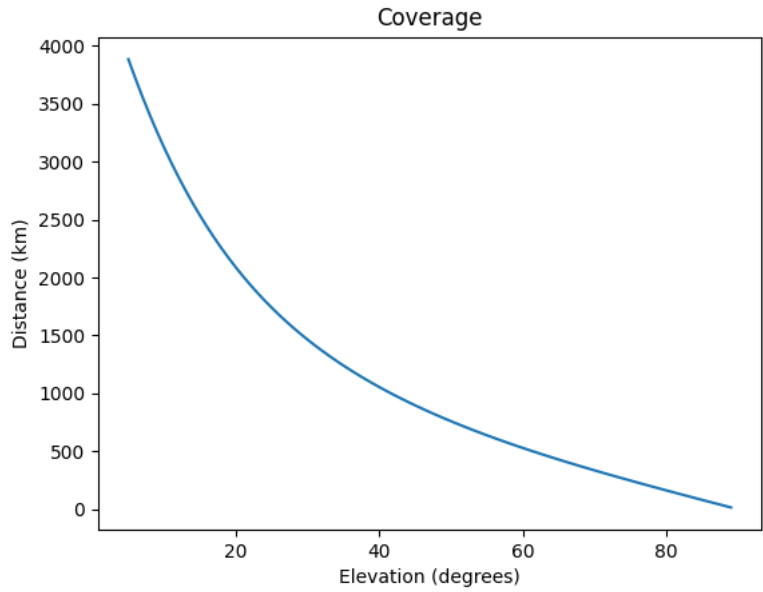


Figure 4.1: Distance covered by a LEO at 500km altitude for different elevation angles

For a High Altitude Platform (HAP) at 20 km altitude the coverage area varies in the following way related to the elevation angle:

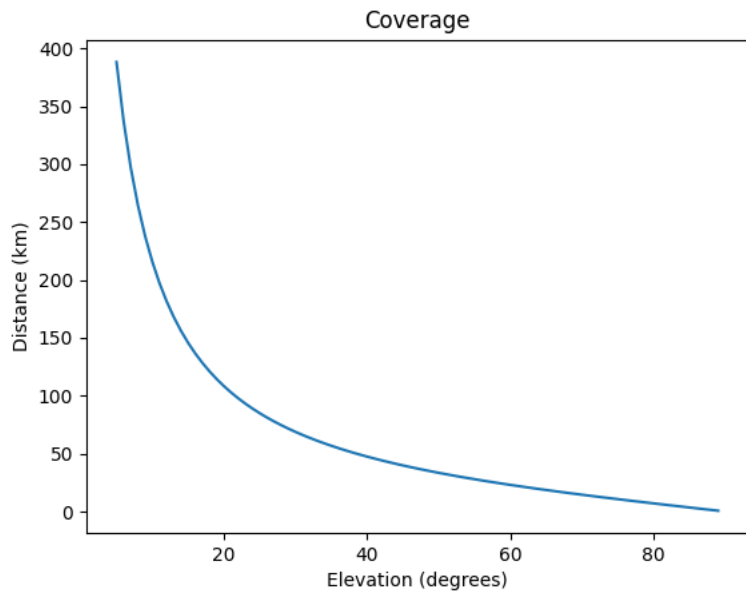


Figure 4.2: Distance covered by a HAP at 20 km altitude for different elevation angles

As we can see from the previous figures obtained with a script in python using the equations from the theoretical overview, the distance covered by a satellite or HAP is highly affected by the elevation angle.

4.2 Link Budget

The BER measurement is an essential aspect to characterize the performance of free space optical communications. For a feasible and reliable link in free space communications a typical minimum value

for the BER for telecommunication applications is around 10^{-9} . Data communications have more stringent requirements where 10^{-13} is often considered minimum. Another important aspect is the Q-factor which describes a qualitative description of the receiver performance because it is a function of the signal to noise ratio (SNR). The Q-factor suggests the minimum SNR required to obtain a specific BER for a given signal. According to [20], taking into account a BER of 10^{-9} for a PPM modulation of order 128, we get a power required at the receiver of around -66 dBm.

During the transmission of information between a transmitter and a receiver using a free space channel, there are many aspects that affect the power of the signal being transmitted. The main aspects that affect the signal transmission are the geometrical losses, related to the misalignment of the beam, the weather losses, related to the weather conditions such as fog, snow and rain, the optical losses related to the optical components of the transceivers being used and the losses due to encounter of the signal with particles with a lower frequency than the signal being used, called Rayleigh Scattering. In the following experiments a wavelength of 850 nm was used. In picture 4.3 we can see how the different type of weather affects the signal being transmitted:

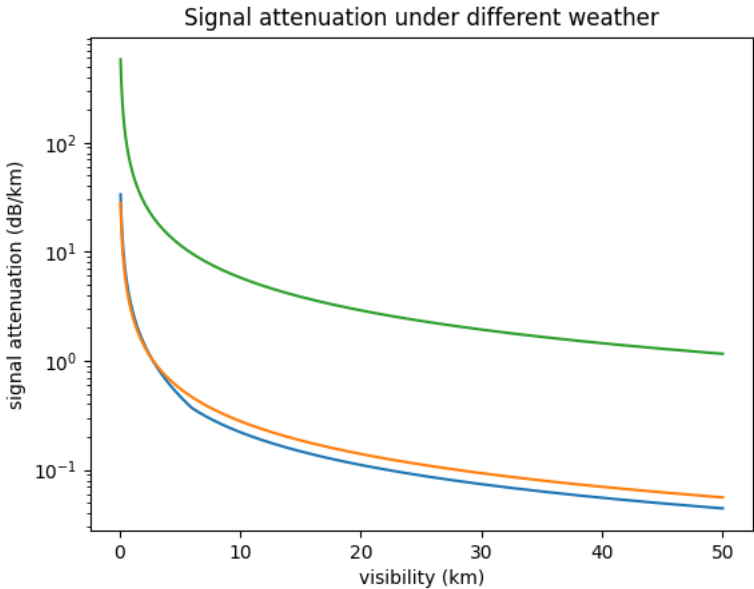


Figure 4.3: Green: Snow; Red: Rain; Blue: Fog

As we can see from the previous graphic, rain and fog have similar effects on the signal transmission whereas snow severely affects the signal, specially if the visibility is low. This means that with extreme weather conditions it is almost impossible to transmit an optical signal through free space since the losses will be too high.

In table 4.2.1 we simulate the values for certain parameters to obtain the link budget for a HAP at 20 km altitude and for a LEO satellite at 500 km altitude

Table 4.2.1 - Link Budget Parameters

Parameter	HAP	LEO satellite
Wavelength	850 nm	850 nm
Fried Parameter	0.2 m	0.2 m
Transmitter Aperture Size	0.1 m	0.1 m
Receiver Aperture Size	0.4 m	0.4 m
Altitude	20 km	500 km
Elevation Angle	5° to 90°	5° to 90°
Weather (Fog/Rain/Snow)	Altitude 5 km	5 km
Rayleigh Losses (L_{atm})	3 dB	3 dB
Losses due to optical components (L_{opt})	6 dB	6 dB
$T_t / T_p / T_r$	0.8	0.8
BER	10^{-9}	10^{-9}
Power Required	-66 dBm	-66 dBm

For a HAP at 20 km altitude with an elevation angle varying from 90 degrees, right at the top of the base station, and 5 degrees, we get a line of sight distance between the base station and the HAP that varies from 20 km at the highest elevation angle to about 230 km at the lowest elevation angle. At these altitudes the main parameters that affect the channel losses have to do with the atmospheric conditions, as shown in the previous graphic, where snow affects the channel the most, making it impossible in some cases to transmit the signal. The value of the wavelength affects mainly the beam divergence angle, which is also affected by the transmitter aperture size, and the atmosphere turbulence induced divergence angle which is also affected by the Fried Parameter that is dependent on the strength of the turbulence. For easier to analyze results we will use typical values for the Fried parameter (r_0), which for wavelengths in the order of 500 nm to 850 nm is around 0.1 m to 0.2 m, decreasing with the strength of the turbulence. The issues involved in the FSO communication in laser uplink are different from the ones suffered in the downlink for LEO satellites, with greater losses related to the beam misalignment on the uplink path. For HAPs since the altitude is around 20 km, the beam on the uplink and downlink will go through the same mean so effects of the turbulence will be similar in both scenarios.

On the other hand for a satellite at 500 km altitude the line of sight distance between the transmitter and receiver can go from 500 km at the highest elevation (90°) angle to 5740 km km at the lowest elevation angle (5°).

For the previous parameters the channel losses, with weather conditions not included) for a HAP at 20 km altitude with different elevation angles, vary in the following way:

As we can see from the previous graphic, the channel losses, non related with the atmospheric

Channel Loss at different LoS distances for H_Hap = 20km (weather conditions not included)

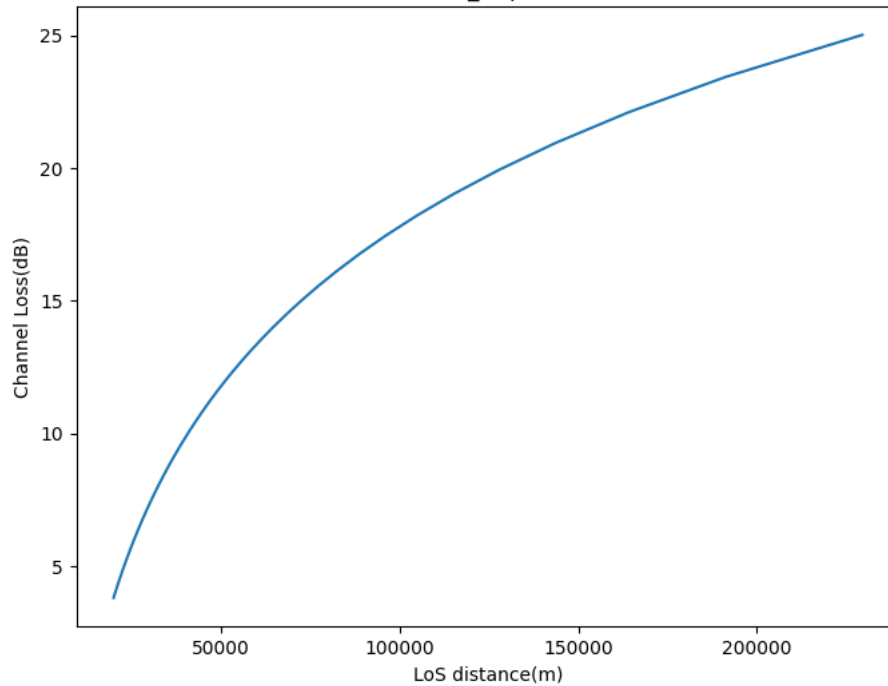


Figure 4.4: Channel loss at different LoS distances (no weather conditions)

conditions, for a HAP at a 20 km altitude can be quite small, going from as low as 7 dBm for the highest elevation angle to around 25 dB at the lowest elevation angle. This means that it is possible to use laser with really low power to transmit the information in the quantum channel. The line-of-sight (LoS) distance is the distance between the transmitter and receiver for the different elevation angles.

Now with the same parameters but for a LEO satellite orbiting at 500 km altitude for different elevation angles and not accounting for the atmospheric losses, the channel losses vary as follows:

Channel Loss at different LoS distances for a LEO sat at 500km (weather conditions not included)

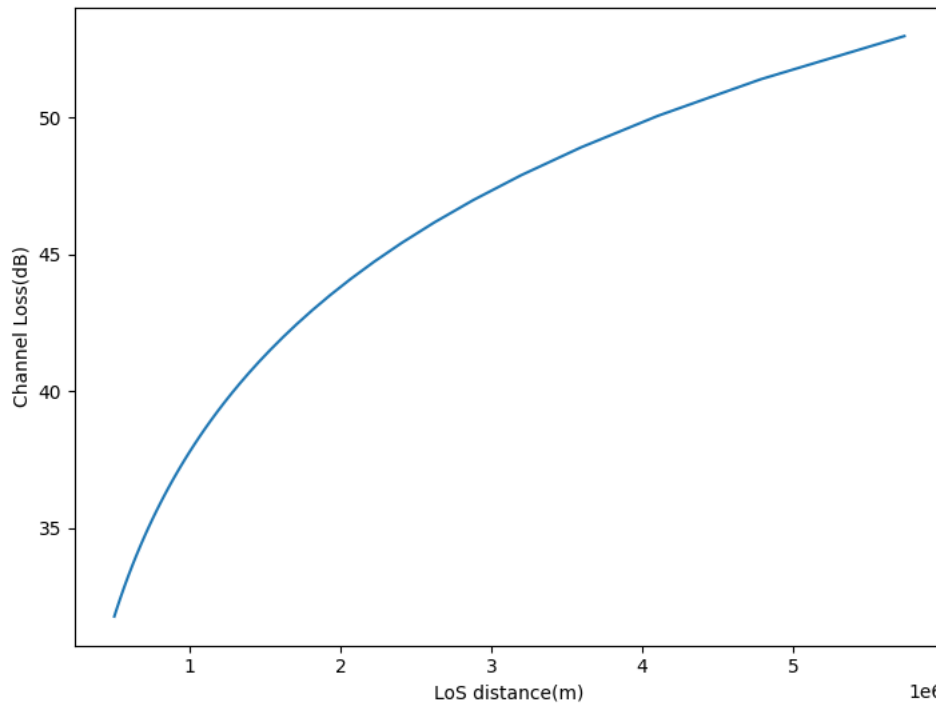


Figure 4.5: Channel loss at different LoS distances (no weather conditions)

As we can see from the previous graphic, the channel losses, non related with the atmospheric conditions, for a LEO satellite at 500 km altitude can go from as low as 30 dB for the highest elevation angle to around 55 dB for the lowest elevation angle. Regarding the photo-detector that could be used, where we used a bit error rate of 10^{-9} which is a common value for digital communications, the minimum power required will be -66 dBm which regarding the channel losses, really low power lasers can be used, such as 5 mW with high margins being achieved.

The attenuation of the channel can also be affected due to physical aspects of the receivers being used and also vary with the wavelength of choice. The previous results were performed for a receiver with a 0.4 m aperture. If instead, for example, a 1 m aperture receiver is used, the total channel attenuation can decrease for around 5 dB for a 500 km distance, and decrease even more for bigger receivers being used. Also higher wavelengths also increase the divergence angle of the laser which result in higher losses at the receiver.

4.3 Pointing System

The pointing system is one the most important aspects in space to Earth communications. Apart from the quantum channel its necessary to have an optical channel that is able to follow the LEO satellite or the HAP in order for the laser to be constantly pointing to the base station. For this situation we have to take into account two parameters: the beam divergence angle and the error or the gimbal being used.

For the type of lasers being used, let's suppose they have a beam divergence angle of about $5 \mu\text{rad}$, which will greatly increase for higher distances, such as the distance between the LEO satellite and the earth station. In the next two graphics we can see how the size of the beam expands for a LEO satellite at 500 km altitude for different elevations angles and for a HAP at 20 km altitude for different elevation angles.

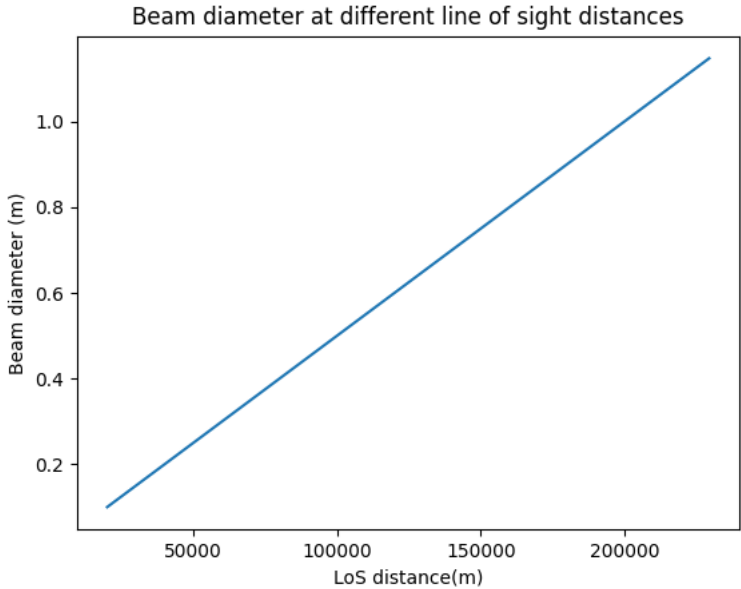


Figure 4.6: Beam diameter at different distances for a HAP

By looking at the previous picture, we can see that for a HAP at 20 km altitude the diameter of the beam at the Earth station goes from 10 cm when the HAP is directly above the station, to about 110 cm when the HAP is at its lowest elevation angle.

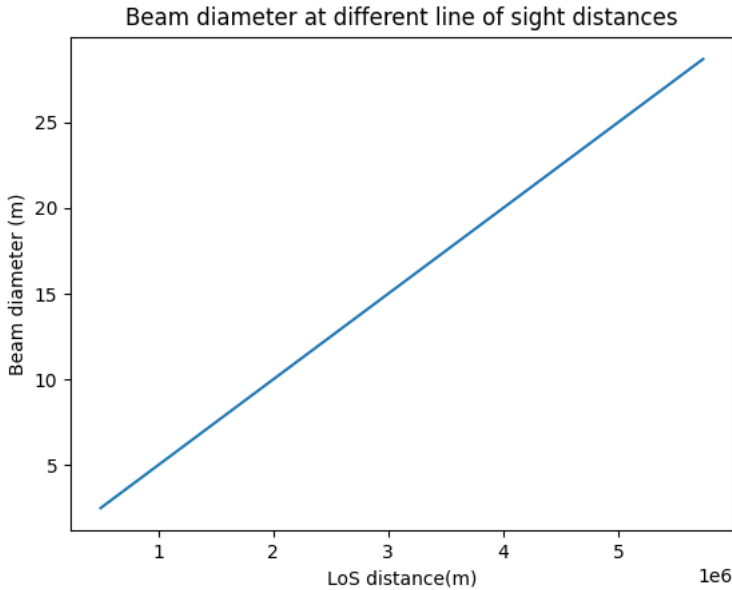


Figure 4.7: Beam diameter at different distances for a LEO

For a LEO at 500 km altitude we can observe that the beam diameter goes from 2.5 m when directly above the Earth station to around 28 m at its highest elevation angle. Allied to this we have to take into account the gimbal where the payload is connected to aboard the LEO satellite or the HAP. Taking into account the gimbal from Foxtech labs, depicted in chapter 3.6 which has an error of 0.01, this means that for for example at a fixed distance of 20 km for a HAP this error can mean that the center of beam at this distance can deviate around 3.5 m, increasing as the distance from the transmitter to the receiver increases resulting in a series of non hits and hits that catch the receiver field of view. This error can be modeled as a gaussian function with a standard deviation of 0.01 and mean value of 0, meaning that there won't be a hit at the receiver for 100 % of times, making the pointing system one of the vital technicalities of satellite free space communication. In the next pictures we can see the maximum displacement of the centroid of the beam for the 0.01 degree error for a HAP at 20 km altitude:

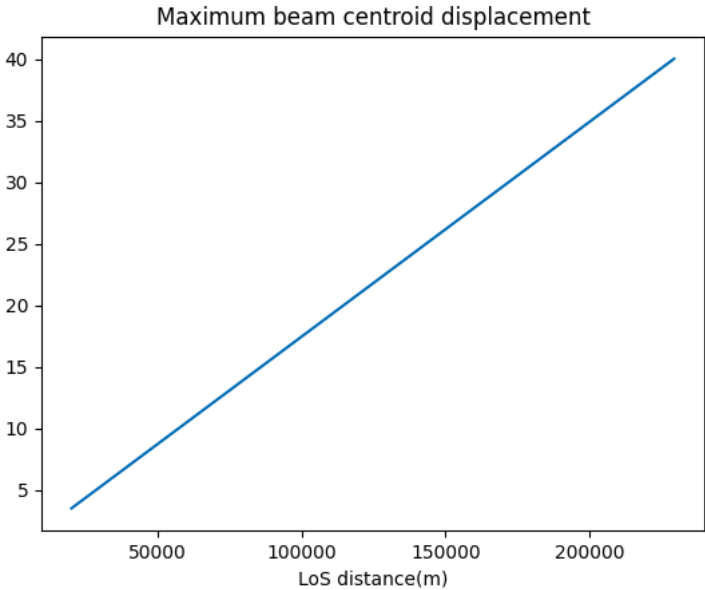


Figure 4.8: Beam centroid displacement at different distances for a HAP

And for a LEO at 500 km distance with different elevation angles the maximum displacement is:

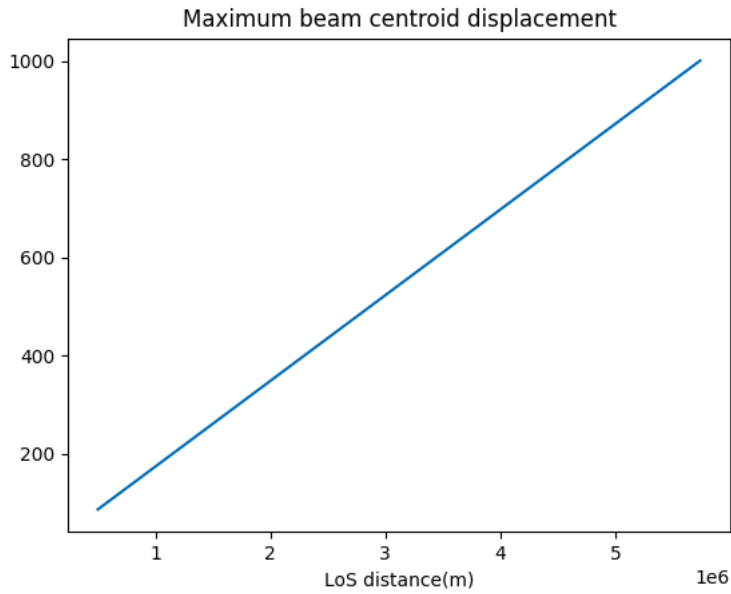


Figure 4.9: Beam centroid displacement at different distances for a LEO

From the pictures we can see that the maximum centroid displacement can go for very high values and will completely miss the receiver. The percentage of hits by the beam on the receiver depends on several parameters such as: the beam divergence angle, which makes the diameter of the beam at the receiver increase with the distance, the gimbal error, which makes the centroid of the beam deviate from its original path, and the size of the receiver. Its possible to make a study about the percentage of hits versus no hits taking into account the previous parameters. In the following graph we can see the percentage of hits for a sample of 200 possible gimbal errors, for a 1 m receiver sizes and at different elevation angles (distances) for a HAP at 20 km altitude.

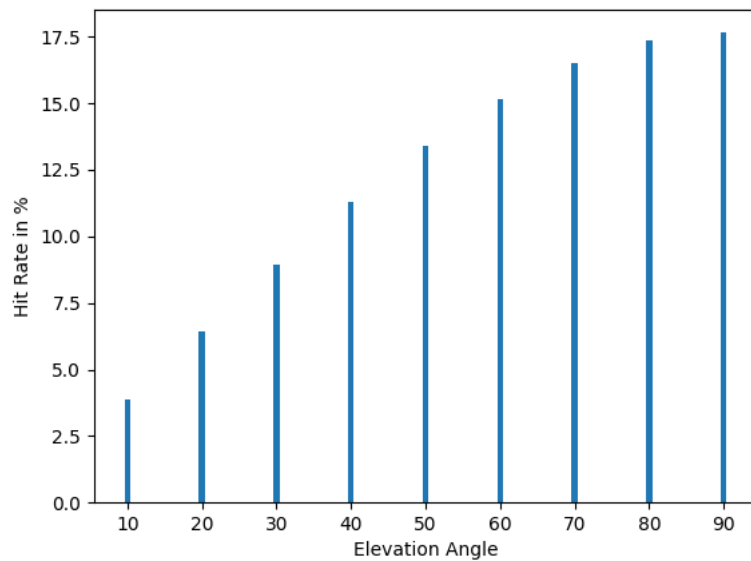


Figure 4.10: Hit rate for a HAP at 20 km altitude and a 1 m aperture receiver

From the previous graphic we can see that the hit rate is much bigger for lower distances between the transmitter and the receiver. It has the same Hit rate for the last two distances due to the fact that the sample used for the gimbal error is not big enough to differentiate those two distances. We can now increase the size of the receiver to 2 m so that we can see the differences in the hit rate.

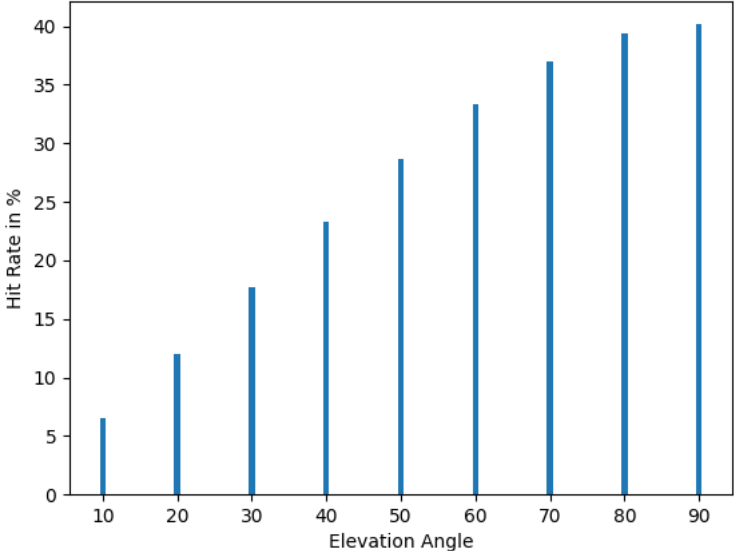


Figure 4.11: Hit rate for a HAP at 20 km altitude and a 2 m aperture receiver

As we can see from the previous graphic, the size of the receiver increases the hit rate for a HAP at 20 km. In the next tables we will see how the same parameters affect a LEO satellite at 500 km altitude and if the parameters also have significant impact on the hit rate. The following graphic shows the hit rate for a LEO satellite at 500 km with a 1 m aperture receiver and a sample for the gimbal error of 10.000 different angles.

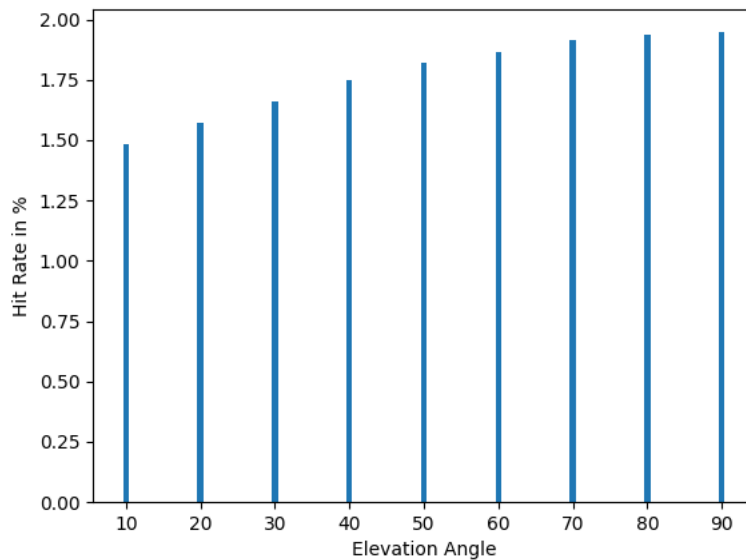


Figure 4.12: Hit rate for a LEO at 500 km altitude and a 1 m aperture receiver

From the previous graphic we see that with this gimbal error for a LEO satellite at 500 km, the hit rate is very low. This means that for the slightest movement of the gimbal, the laser will most likely miss the receiver. Now with the same parameters but for a 2 m receiver.

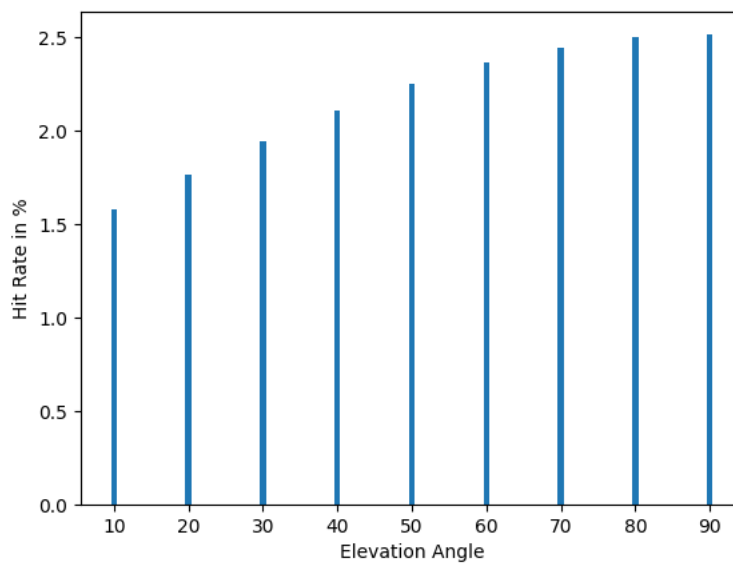


Figure 4.13: Hit rate for a LEO at 500 km altitude and a 2 m aperture receiver

From the previous values we understand that the receiver size is a very important aspect when it comes to having a higher data rate. From all the results gathered, when comparing a HAP at 20 km altitude with a LEO satellite at 500 km, we can see that a gimbal with a 0.01 error and a receiver with a decent size is more than enough to have a good hit rate on a HAP, with the hit rate increasing with bigger receivers. As for the satellite, this gimbal might not be the best solution since the satellite can be at distances much greater than the HAP, where a small error from the gimbal in that interval means a

very high error at the Earth, making the beam completely miss the receiver.

4.4 Benchmarking

On this chapter I will study the link budget analysis using different methods by different authors in order to compare the final results and check if the model that we use is feasible or not.

Table 4.4.1 - Link Budget Parameters

Parameters	Nano Losses(Method 1)	Total Losses(Method 2)
Wavelength	1550nm	1550nm
Fried Parameter	0.2m	0.2m
Transmitter Aperture Size	0.1m	0.1m
Receiver Aperture Size	0.4m	0.4m
Hap Altitude	20km	20km
HAP Elevation Angle	5° to 90°	5° to 90°
Weather Altitude (Fog/Rain/Snow)	5km	5km
Rayleigh Losses (L_{atm})	3dB	3dB
Losses due to optical components (L_{opt})	6dB	6dB
$T_t / T_p / T_r$	0.8	0.8
Transmitting Power	10 mW	10 mW
Divergence of pointing jitter (θ_j)	5 μ rad	5 μ rad

The first model that we are taking as a reference for the Link budget analysis on HAP's is the NanoBob method which is implemented in [1] In this method the losses are given by:

$$L_{Nano} = 10 \log_{10} \left(\frac{R_{Los}^2 (\theta^2 + \theta_{atm}^2)}{D_{rx}^2 + T_t T_p T_r} \right) + L_{atm} + L_w R_w + L_{opt} \quad (4.1)$$

As described in section 3.5.

The authors use a second method to make comparisons with the results obtained from the NanoBob method. Where the losses are given by:

$$L_T = L_p + L_{geo} + L_{ma} R_{LoS} + L_w R_w + L_{rx} \quad (4.2)$$

In the next table we can see the differences in the Power at the receiver using both methods and not taking the atmospheric attenuation due to weather into consideration since the attenuation will be the same in both cases. The main differences between the methods is the way the beam divergence,

the atmosphere turbulence included divergence angle and the size of the receiver and transmitter are implemented in the equations.

Table 4.4.2 - Total Losses

LoS Distance(km)	Total Losses NanoBob method (dB)	Total Losses method 2 (dB)	P_R (dBm) (NanoBob)	P_R (dBm) (Method 2)
20	10	9	0	1
50	18	16	-9	-6
75	22	20	-12	-10
100	24	21	-14	-11
125	26	24	-16	-14
150	27	26	-17	-16
175	28	28	-19	-18
200	30	30	-20	-20

As we can see from the previous table the channel losses for both models are very similar, with NanoBob having a slight increase along the link range mainly because of the overestimated beam divergence.

In the next method, used by [29] the Power received is expressed as:

$$P_r = \frac{A_r}{\pi \frac{\theta L^2}{2}} \cdot T \cdot 10^{\frac{-\alpha L}{10}} \cdot P_t + P_{bg} \quad (4.3)$$

Where α , T and A_r are the atmospheric attenuation, combined transmitter receiver optical efficiency and receiver aperture area, respectively. P_r , P_t and P_{bg} are the received optical power, transmitted optical power and background optical noise, respectively. Using the same parameters as the previous two models and not accounting for the atmospheric attenuation nor the background noise:

Table 4.4.3 - Total Losses

<i>LoS</i> Distance(km)	Total Losses without weather(dB)	$P_r(mW)$	$P_R(dBm)$
20	43	3×10^{-4}	-35
50	51	5×10^{-5}	-43
75	55	2×10^{-5}	-46
100	58	1.4×10^{-5}	-48
125	60	1×10^{-5}	-50
150	61	8×10^{-6}	-51
175	63	4×10^{-6}	-54
200	64	3×10^{-9}	-90

From the table above the results obtained with this model are not very similar with the ones obtained from the "Feasibility of Quantum Key Distribution from high altitude platforms", where we have lower attenuation for longer link distances. In this model the tests were made for a 1 km distance.

In the following study performed by [30] the author presents a link budget corresponding to a system consisting of a fiber amplifier transmitter and an APD detector providing a M-ary PPM communication Link. For the transmitter parameters the author uses a laser followed by an average-power limited erbium-doped fiber amplifier (EDFA) which produces a 200 mW at 1550 nm. An additional 3 dB of transmitter losses are included to account for implementation losses. For the channel parameters the LEO is at a 400 km altitude which with a 20 ° elevation angle corresponds to a 1000 km path length. The author uses the standard free space losses equation to account for diffraction loss. According to predictions from the model used by the author he uses 1 dB for atmospheric losses. He assumes a fixed pointing loss of 3dB as a result of a requirement placed on the pointing subsystem. For the receiver parameters a 30 cm aperture telescope is used at the base station with 2 dB coupling losses. The receiver sensitivity analysis accounts for both shot noise as well as detector noise. The received power is the transmitted power plus gains from transmit and receive telescopes minus the losses from various sources.

$$P_{rec} = P_T + G_T + G_R - L_T - L_R - L_{FS} - L_{atm} - L_{pointing} \quad (4.4)$$

The author Link Budget Summary for a 1000 km link distance is as follows:

Table 4.4.4 - Link Budget Summary

Link Budget Summary	Values (dB)
Laser avg. optical power	-7
Transmitter optical losses	-1.5
Transmitter antenna gain	65.6
Path Loss	-258
Atmospheric loss	-1
Pointing loss	-3
Receiver antenna gain	115
Receiver optical losses	-2
Power received	-91 dBm

Using the same parameters but for a HAP at 20 km altitude and for a 10 mW transmitting power we get:

Table 4.4.5

LoS distance (km)	$P_R(dBm)$
20	-40.4
50	-46
75	-50
100	-53
125	-55
150	-57
175	-59
200	-60

In [20] they want to successfully establish a communication link between Earth and a LEO satellite at a maximum link distance of 1000 km. The received power at the detector on the ground terminal has to be estimated when 200 mW of average power is being transmitted by the NOCT onboard satellite. The authors calculate the required optical power at the detector for a target BER of 10^{-5} for an uncoded system. The authors calculate the link parameters for a high data rate, 50 Mbps, which is achieved using 16 PPM and a lower data rate of 10 Mbps which is achieved using a more power-efficient 128 PPM. Higher data rates will need a bigger telescope, for example 1 m for 16 PPM. The main differences between the link design for both techniques are the requirement of receiver size, receiver antenna gain, power of the signal at the receiver and the power required at the receiver for a certain BER. The link parameters used by authors are the following:

Table 4.4.6

Parameter	128 PPM	16 PPM
Data Rate (MPS)	10	50
BER	10^{-5}	10^{-5}
Receiver antenna size(cm)	25.4	100
Laser avg. opt. power (dBm)	23.1	23.1
Transmitter optical losses(dB)	-1.5	-1.5
Transmitter antenna Gain (dBi)	64.96	64.96
Path Loss (dB)	-258.2	-258.2
Atmospheric Loss (dB)	-1	-1
Pointing loss (dB)	-3	-3
Receiver antenna gain (dBi)	114.26	126
Receiver optical losses (dB)	-2.5	-2.5
Signal Power at detector (dBm)	-63.98	-52.24
Signal Power required (dBm)	-67.5	-59
Margin (dB)	3.52	6.76

The authors use the equations that are described in this chapter 3.4 about the BER for PPM modulation to compute the BER with varying received power for each PPM order. They concluded that for the 16 PPM the minimum BER is achieved for a -59 dBm input power, whereas for the 128 PPM the required BER is achieved for a lower input of -67 dBm.

Taking into account all the methods chosen to compare the Link Budget, all the methods have similar results regarding the losses on the optical channel.

Chapter 5

Conclusions

In this thesis the characteristics and properties of free space optical communications were studied along with the main challenges of having a QKD system on a LEO satellite or on a HAP in space, regarding the SWAP (size, weight and power) of a possible payload, the atmospheric turbulence that deviates the beam from its original path, the atmospheric conditions that affect the availability and the power of the signal received, the possible area covered by these two systems, and the need for an accurate acquisition, tracking and pointing system. These while comparing both LEO satellites and HAPs. LEO satellites and HAPs have different purposes and so different characteristics. Regarding the coverage area, a LEO satellite has a much bigger footprint than a HAP, which means that a HAP can only be used in small regions whereas a satellite can be used for much larger coverage. HAPs are also much cheaper to deploy than a LEO satellite, and since their deployments are at lower altitudes, its possible to have favourable link budgets with higher SNR. Another important aspect is the orbital velocity, since a HAP can be almost stationary where on the contrary a LEO satellite has a big orbital velocity, the signal availability varies in both situations.

Regarding the coverage area, which greatly depends on the altitude, we observed that a HAP can cover a point to point distance from 20 km at its highest elevation angle to around 250 km at an elevation angle of about 10° . Lower elevation angles have a bigger footprint but can suffer interference from buildings and other high structures on Earth. Regarding the LEO satellite, the coverage footprint is much bigger. Orbiting at 500 km, a LEO satellite can cover distances from around 500 km when directly above the Earth station to distances around 3500 km for the lowest elevation angles. Considering these different footprints, LEO satellites are used more for global coverage where HAPs are more used for local coverage of small areas.

At the receiver side the most commonly used photodetectors in optical communications are the photodiodes. APD's are the most used in the photodetection process because they have high sensitivity, fast response time, small size and low cost. The performance of the optical receiver in a digital transmission system is measured by the Bit Error Rate (BER). The BER is defined as the ratio between the number of incorrectly detected bits and the total number of bits transferred in a given time interval. BER can be calculated using different types of modulation, The two most used types of modulation in free

space optics are the OOK modulation and the PPM modulation. Different BER's imply different powers required at the receiver, which is essential to understand the characteristics of the system. In optical communications a BER of 10^{-9} is usually used.

The two most common noise sources that affect the SNR are the shot noise, also called quantum noise, and the circuit noise. The presence of noise limits the ability of the receiver to detect an incoming signal. The SNR is also affected by the degradation of the optical signal travelling through the atmospheric channel.

The pointing system is one of the biggest challenges in space optical communications. In a payload, apart from the quantum system, there needs to be a classical system in order to be able to constantly guide the laser between the satellite and the Earth station. For a HAP, the ATP (acquisition, tracking and pointing) process is simpler because it is quasi stationary. Nevertheless, the random variations on the platform can deviate the signal from its original path. These variations can be corrected by using a gimbal which will still have an error that we have to account for. This gimbal error follows a gaussian distribution and inevitably will make the beam miss the Earth station in a certain percentage of times, making the signal unavailable. On a HAP, since the distance between the HAP and the Earth station is small compared to the distance from the LEO satellite to the station, on the HAP we can discard the losses due to the misalignment of the beam regarding the turbulent atmosphere. On the other hand for a LEO satellite, this misalignment losses regarding the turbulence have to be taken into account for an uplink connection because after going through a turbulent environment for about 20 km, it will travel a further distance to get to the satellite, where the misalignment of the laser will have a much greater impact. For a LEO satellite the gimbal studied in this thesis might not be appropriate because a 0.01° error at such great distances will imply a big variation on the centroid of the beam. Usually for this type of satellites they use their own ADCS (attitude determination and control system). As we saw from the results about the pointing and the gimbal error, a HAP at 20 km can have a high data rate with increasingly higher hit rates for bigger receivers, which is a possibility for downlinks. For a 1 m receiver, a HAP can have a hit rate as low as 3.7% for the lowest elevation angle (longest distance) and a 17.7% hit rate for the highest elevation angle (shortest distance). Whereas if a 2 m receiver is used, the hit rate can vary between 6.3% and 40.5%, which is a dramatic increase when compared to a receiver with half the size. As for a LEO satellite, the hit rate for a 1 m receiver went from 1.5% to 1.9% and for a 2 m receiver from 1.6% to 2.5%. Despite the increase, the hit rate is still very low, which means that this gimbal can be a good match for a platform at low altitudes but for a LEO at 500 km altitude there should be a better pointing system with a smaller error.

Regarding the link budget, there are several aspects that affect the link channel. The choice of the wavelength can increase or decrease the losses. Lower frequencies imply a higher divergence angle of the laser which means less power arriving at the receiver. The atmospheric conditions is what affects the signal the most. Rain and fog affect the signal almost in the same way, whereas snow can severely affect the visibility and therefore making the signal completely unavailable. For LEO satellites, as mentioned before, in the uplink, the misalignment of the beam due to atmospheric turbulence is one of the main sources of link losses. Apart from this, the receiver aperture size can also decrease the losses in the

path regarding the misalignment. In this case its possible to have bigger receivers for downlinks than it is for uplinks, due to the SWAP (size, weight and power) constraints of the satellite. There are other physical aspects that introduce losses in the link that have to do with the optical components used in the transmitters and receivers.

Bibliography

- [1] Y. Chu, R. Donaldson, R. Kumar, and D. Grace. Feasibility of quantum key distribution from high altitude platforms. *Quantum Science and Technology*, 2021.
- [2] D. L. Begley. Free-space laser communications: a historical perspective. In *The 15th Annual Meeting of the IEEE Lasers and Electro-Optics Society*, volume 2, pages 391–392. IEEE, 2002.
- [3] B. Furch, Z. Sodnik, and H. Lutz. Optical communications in space—a challenge for europe. *AEU-International Journal of Electronics and Communications*, 56(4):223–231, 2002.
- [4] A. Carrasco-Casado and R. Mata-Calvo. *Space Optical Links for Communication Networks*, pages 1057–1103. Springer International Publishing, Cham, 2020. ISBN 978-3-030-16250-4. doi: 10.1007/978-3-030-16250-4_34. URL https://doi.org/10.1007/978-3-030-16250-4_34.
- [5] C. H. Bennett, F. Bessette, G. Brassard, L. Salvail, and J. Smolin. Experimental quantum cryptography. *Journal of cryptology*, 5(1):3–28, 1992.
- [6] T. Bisztray and L. Bacsardi. The evolution of free-space quantum key distribution. *Infocommunications Journal*, 10(1):22–30, 2018.
- [7] B. Jacobs and J. Franson. Quantum cryptography in free space. *Optics Letters*, 21(22):1854–1856, 1996.
- [8] R. Ursin, F. Tiefenbacher, T. Schmitt-Manderbach, H. Weier, T. Scheidl, M. Lindenthal, B. Blauensteiner, T. Jennewein, J. Perdigues, P. Trojek, et al. Free-space distribution of entanglement and single photons over 144 km. *arXiv preprint quant-ph/0607182*, 2006.
- [9] R. F. Werner. Quantum states with einstein-podolsky-rosen correlations admitting a hidden-variable model. *Physical Review A*, 40(8):4277, 1989.
- [10] J.-P. Bourgoin, B. L. Higgins, N. Gigov, C. Holloway, C. J. Pugh, S. Kaiser, M. Cranmer, and T. Jennewein. Free-space quantum key distribution to a moving receiver. *Optics express*, 23(26):33437–33447, 2015.
- [11] P. Jianwei. Progress of the quantum experiment science satellite (quess) micus project. , 38(5): 604–609, 2018.

- [12] A. Carrasco-Casado, H. Takenaka, D. Kolev, Y. Munemasa, H. Kunimori, K. Suzuki, T. Fuse, T. Kubo-Oka, M. Akioka, Y. Koyama, et al. Leo-to-ground optical communications using sota (small optical transponder)–payload verification results and experiments on space quantum communications. *Acta Astronautica*, 139:377–384, 2017.
- [13] H. Podmore, I. D’Souza, D. Hudson, T. Jennewin, J. Cain, B. Higgins, C. Midwinter, A. Scott, A. McColgan, D. Caldwell, et al. Optical terminal for canada’s quantum encryption and science satellite (qeysat). In *2019 IEEE International Conference on Space Optical Systems and Applications (ICSOS)*, pages 1–5. IEEE, 2019.
- [14] C. Pollier. System design and orbit analysis for spooqsat-1. 2016.
- [15] R. Bedington, E. Truong-Cao, Y. Tan, C. Cheng, K. Durak, J. Grieve, J. Larsen, D. Oi, and A. Ling. Deploying quantum light sources on nanosatellites ii: lessons and perspectives on cubesat spacecraft. In *Electro-Optical and Infrared Systems: Technology and Applications XII; and Quantum Information Science and Technology*, volume 9648, page 964811. International Society for Optics and Photonics, 2015.
- [16] E. Kerstel, A. Gardelein, M. Barthelemy, M. Fink, S. K. Joshi, and R. Ursin. Nanobob: a cubesat mission concept for quantum communication experiments in an uplink configuration. *EPJ Quantum Technology*, 5(1):6, 2018.
- [17] S. Cakaj, B. Kamo, A. Lala, and A. Rakipi. The coverage analysis for low earth orbiting satellites at low elevation. *International Journal of Advanced Computer Science and Applications*, 5(6), 2014.
- [18] J. Guimarães, M. J. Martins, and A. Baptista. Optical inter-satellite links: Applications in defense. *PROELIUM*, 7:361–379, 2016.
- [19] J. Oscarsson. Simulation of optical communication for formation flying spacecraft. *no. April*, page 95, 2008.
- [20] N. Singh, R. Keshavappa, A. Dixit, S. b Umesh, et al. Design of transmitter communication module for nanosatellite optical communication terminal. In *2020 IEEE International Conference on Advanced Networks and Telecommunications Systems (ANTS)*, pages 1–6. IEEE, 2020.
- [21] W.-C. Wang. Optical detectors. *Department of Power Mechanical Engineering, National Tsing Hua University*. <https://depts.washington.edu/micttech/optics/me557/detector.pdf>, 12, 2011.
- [22] G. K. Kurt, M. G. Khoshkholgh, S. Alfattani, A. Ibrahim, T. S. Darwish, M. S. Alam, H. Yanikomeroglu, and A. Yongacoglu. A vision and framework for the high altitude platform station (haps) networks of the future. *IEEE Communications Surveys & Tutorials*, 23(2):729–779, 2021.
- [23] O. Čierný. Precision closed-loop laser pointing system for the nanosatellite optical downlink experiment, 2017.

- [24] M. Pfennigbauer, M. Aspelmeyer, W. Leeb, G. Baister, T. Dreischer, T. Jennewein, G. Neckamm, J. Perdigues, H. Weinfurter, and A. Zeilinger. Satellite-based quantum communication terminal employing state-of-the-art technology. *Journal of Optical Networking*, 4(9):549–560, 2005.
- [25] K. Cahoy, P. Grenfell, A. Crews, M. Long, P. Serra, A. Nguyen, R. Fitzgerald, C. Haughwout, R. Diez, A. Aguilar, et al. The cubesat laser infrared crosslink mission (click). In *International Conference on Space Optics—ICSO 2018*, volume 11180, page 111800Y. International Society for Optics and Photonics, 2019.
- [26] D. Bouwmeester and A. Zeilinger. The physics of quantum information: basic concepts. In *The physics of quantum information*, pages 1–14. Springer, 2000.
- [27] L. Mazzarella, C. Lowe, D. Lowndes, S. K. Joshi, S. Greenland, D. McNeil, C. Mercury, M. Macdonald, J. Rarity, and D. K. L. Oi. Quarc: quantum research cubesat—a constellation for quantum communication. *Cryptography*, 4(1):7, 2020.
- [28] O. Lee and T. Vergoossen. An updated analysis of satellite quantum-key distribution missions. *arXiv preprint arXiv:1909.13061*, 2019.
- [29] M. B. Awan and S. Mohan. Analysis of beam divergence and input bit rate for free space optical communication link. In *2016 IEEE 37th Sarnoff Symposium*, pages 83–87. IEEE, 2016.
- [30] R. W. Kingsbury. *Optical communications for small satellites*. PhD thesis, Massachusetts Institute of Technology, 2015.

